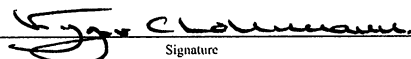Author

Matthew S. Wasson

Title

ISOTOPIC AND ELEMENTAL EVIDENCE FOR METEORIC ALTERATION WITHIN A PENNSYLVANIAN PHYLLOID-ALGAL MOUND, HOLDER FORMATION, NEW MEXICO

submitted in partial fulfillment
of the requirements for the degree of
Master of Science in Geology
Department of Geological Sciences
The University of Michigan

Accepted by:

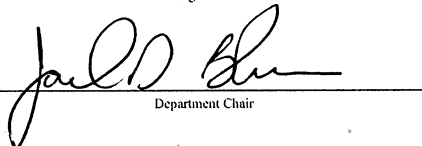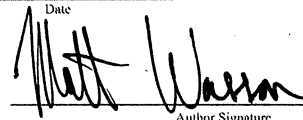|		
Signature	Kyger C Lohmann _Name_	12-08-2005 _Date_
Signature	Bruce H. Wilkinson _Name_	12-8-05 _Date_
Department Chair	Joel D. Blum _Name_	12-12-05 _Date_

I hereby grant the University of Michigan, its heirs and assigns, the non-exclusive right to reproduce and distribute single copies of my thesis, in whole or in part, in any format. I represent and warrant to the University of Michigan that the thesis is an original work, does not infringe or violate any rights of others, and that I make these grants as the sole owner of the rights to my thesis. I understand that I will not receive royalties for any reproduction of this thesis.

☒ Permission granted.

☐ Permission granted to copy after: _____ Date

☐ Permission declined.

Author Signature

ISOTOPIC AND ELEMENTAL EVIDENCE FOR METEORIC

ALTERATION WITHIN A PENNSYLVANIAN PHYLLOID-ALGAL

MOUND, HOLDER FORMATION, NEW MEXICO

Matthew S. Wasson
December, 2005

ACKNOWLEDGEMENTS

ABSTRACT

Yucca Mound, a Virgilian (late Pennsylvanian) phylloid-algal bioherm exposed in the Sacramento Mountains of south-central New Mexico developed on a shallow shelf off the Pedernal landmass. The bioherm contains two distinct exposure surfaces identified by the presence of red/orange oxidized zones and features associated with soil formation. Stratigraphically, there is one subaerial exposure surface within the mound and another that caps the unit. Through petrographic and geochemical analysis five low-Mg calcite cement phases have been identified that occlude most primary and secondary porosity.

Correlation of exposure surfaces and cement phases demonstrates that this mound experienced two distinct episodes of meteoric diagenesis. As meteoric water initially passed through the bioherm, during relative sea-level fall and development of the first exposure surface, considerable porosity was created through the dissolution of aragonitic allochems. Early, during the first period of exposure, meteoric/marine mixing is evident with precipitation of early Cement I, characterized by a mottled cathodoluminescent microfabric and displaying a higher Mg content and more positive $\delta^{18}O$ values than late Cement I precipitates, which formed as sea-level continued to fall. Late Cement I, interpreted to have formed from meteoric water, has an average $\delta^{18}O_{VPDB} = -4.8‰$. Relative sea-level then rose and marine waters once again inundated the mound and flanking facies. A second episode of subaerial exposure is manifested by development of a soil zone and precipitation of calcite Cement II and Cement III ($\delta^{18}O_{VPDB} = -5.6‰$). This is followed by Cement IV, most likely precipitated in an increasingly reducing system, under shallow burial, due to a decrease in

permeability, from interstitial waters that remained after the second stage of meteoric diagenesis. Remaining porosity was occluded by calcite Cement V which was precipitated from connate waters during a later stage of burial.

Numerical modeling of observed Mg, Sr, and $\delta^{13}C$ values shows that R/W ratios during both stages of meteoric diagenesis were exceedingly low (maximum of 0.0057). This modeling also implies that the initial mound carbonate Sr concentration ranged from 1,300 to 5,000 ppm (0.1-0.5 mole%), with a Mg concentration from 7,000 to 30,000 ppm (4-12 mole%), which suggests that the original mineralogy of the mound facies was a mixture of aragonite and high-Mg calcite.

INTRODUCTION

This study focuses on patterns of meteoric diagenesis in biohermal, interbiohermal, and flanking facies of the Lower Holder Formation exposed in the Sacramento Mountains of New Mexico (Figures 1, 2, & 3). Through petrographic analysis, the sequence of cementation was identified based on distinct cathodoluminescent characteristics and pore-filling relationships that serve as a record of the alteration history of the unit. By coupling petrographic data with geochemical analysis of the cements and other rock constituents, a paragenetic sequence was constructed that allows for the development of a relative chronology among the various diagenetic stages. From this, the depositional, exposure, and subsidence histories of the unit have been reconstructed.

Identification of surfaces of subaerial exposure diagenesis in carbonate sequences based on geochemical proxies is not a new concept. Since the pioneering work by Allan and Matthews (1982) to more recent analyses by Saller and Moore (1991), Tobin et al. (1999), and Benito et al. (2001), the geochemical signature of exposure surfaces has been fairly well established. Most studies, however, assume that the bulk of porosity is created by a single stage of meteoric diagenesis, and is subsequently occluded by cement precipitated from these waters. Only a few studies have been able to document multiple stages of meteoric diagenesis from within a continuous sequence of cements (Benito et al., 2001; Moldovanyi and Lohmann, 1984), by employing microsampling techniques to validate the multiple episodes of meteoric diagenesis. In contrast, the majority of prior studies have been based on whole rock analysis in which the various constituents of a sample, such as cement, allochems, or

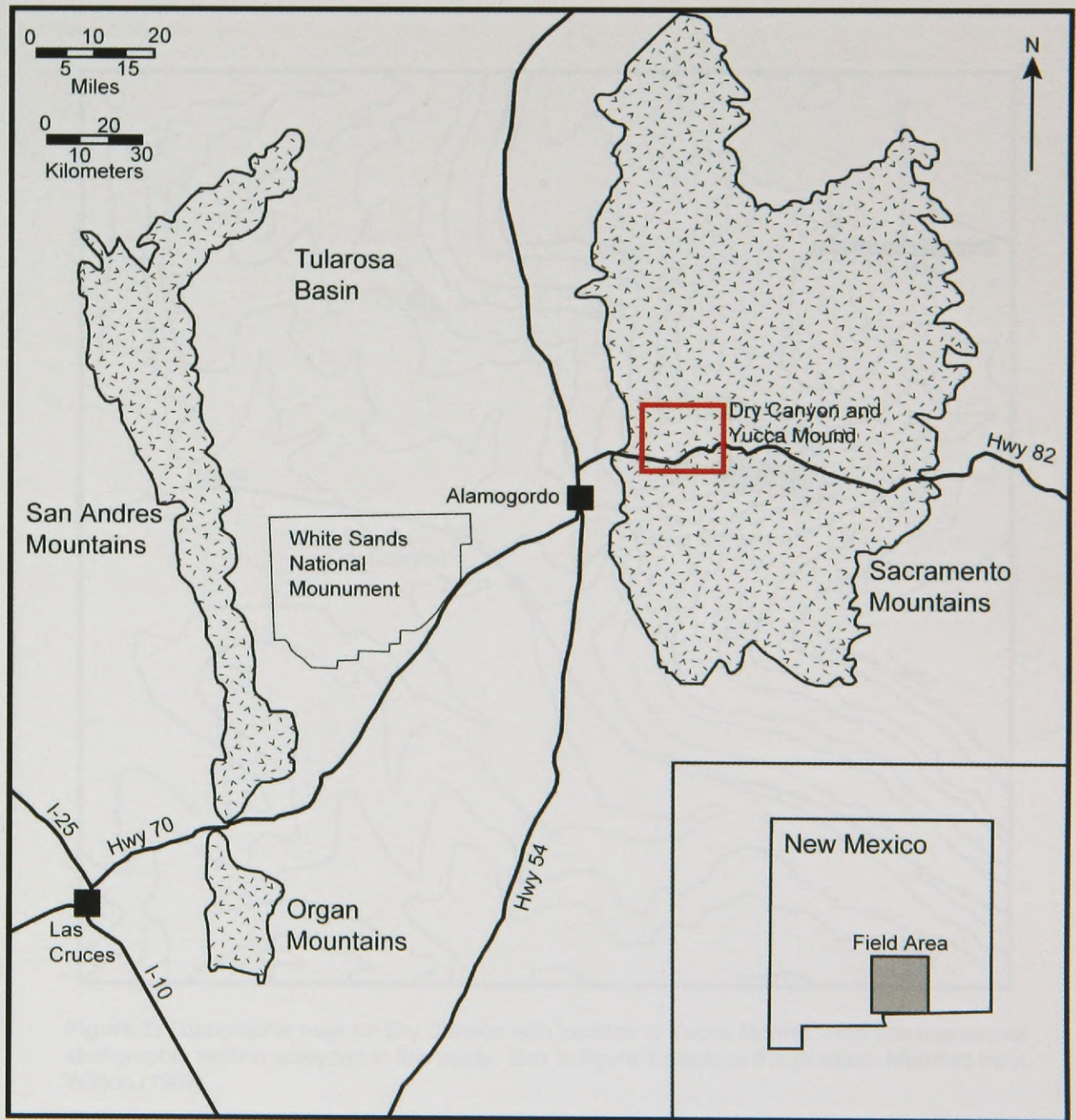**Figure 1:** Map of south-central New Mexico showing locations of major mountain ranges, cities and roads. Field area highlighted with a box. Modified from Rivera (1999) and Algeo et al. (1991).
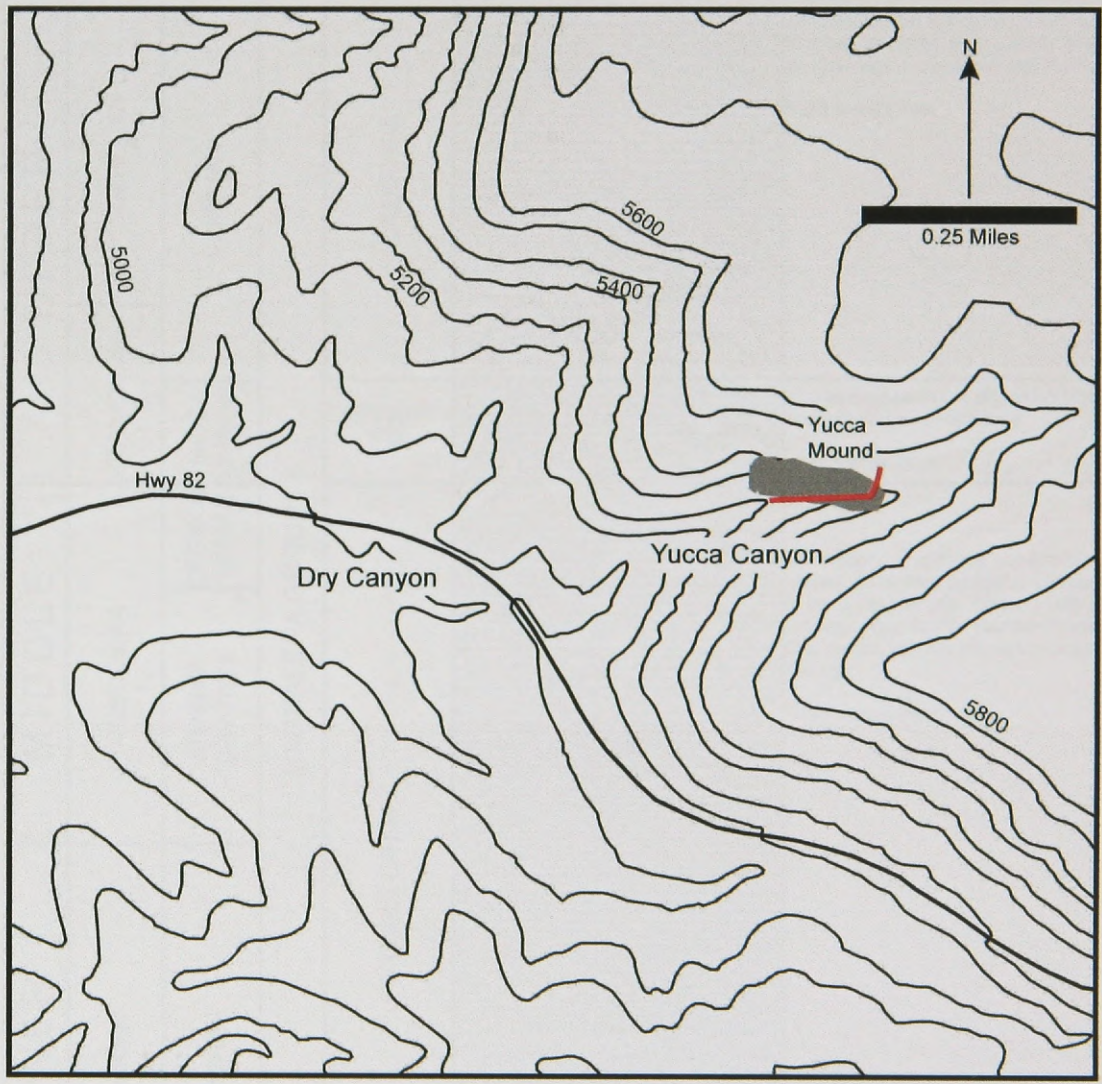
Figure 2: Topographic map for Dry Canyon with location of Yucca Mound. Red line represents stratigraphic section analyzed in this study. Box in figure 1 displays this location. Modified from Wilson (1967).

System	Series	Stage		SACRAMENTO MOUNTAINS		Lithology

The figure shows a stratigraphic column with the following text labels:

System: PENNSYLVANIAN
Series: UPPER, MIDDLE, LOWER
Stage: GZHELIAN, KASIMOVIAN, MOSCOVIAN, BASHKIRIAN (ICS); VIRGILIAN, MISSOURIAN, DESMOINESIAN, ATOKAN/DERRYAN, MORROWAN (North American)
Sacramento Mountains: MAGDALENA GROUP — HOLDER FM., BEEMAN FM., GOBBLER FM.

Age markers: 299.0 Ma, 306.5, 311.7, 318.1 Ma

North — South

Lithology descriptions:

Dominantly limestone with interbedded sandstones and shales along with sparse channel conglomerates. Locally developed phylloid-algal mounds towards the base.
~275 meters thick

Interbedded shales, argillaceous limestones and thin arkosic sandstones.
~150 meters thick

Interbedded limestones, sandstones and shales; dominated by coarse sandstone in the lower portions. Massive gray cherty limeston (Bug Scuffle Member) towards top that grades laterally into sandstones and shales.
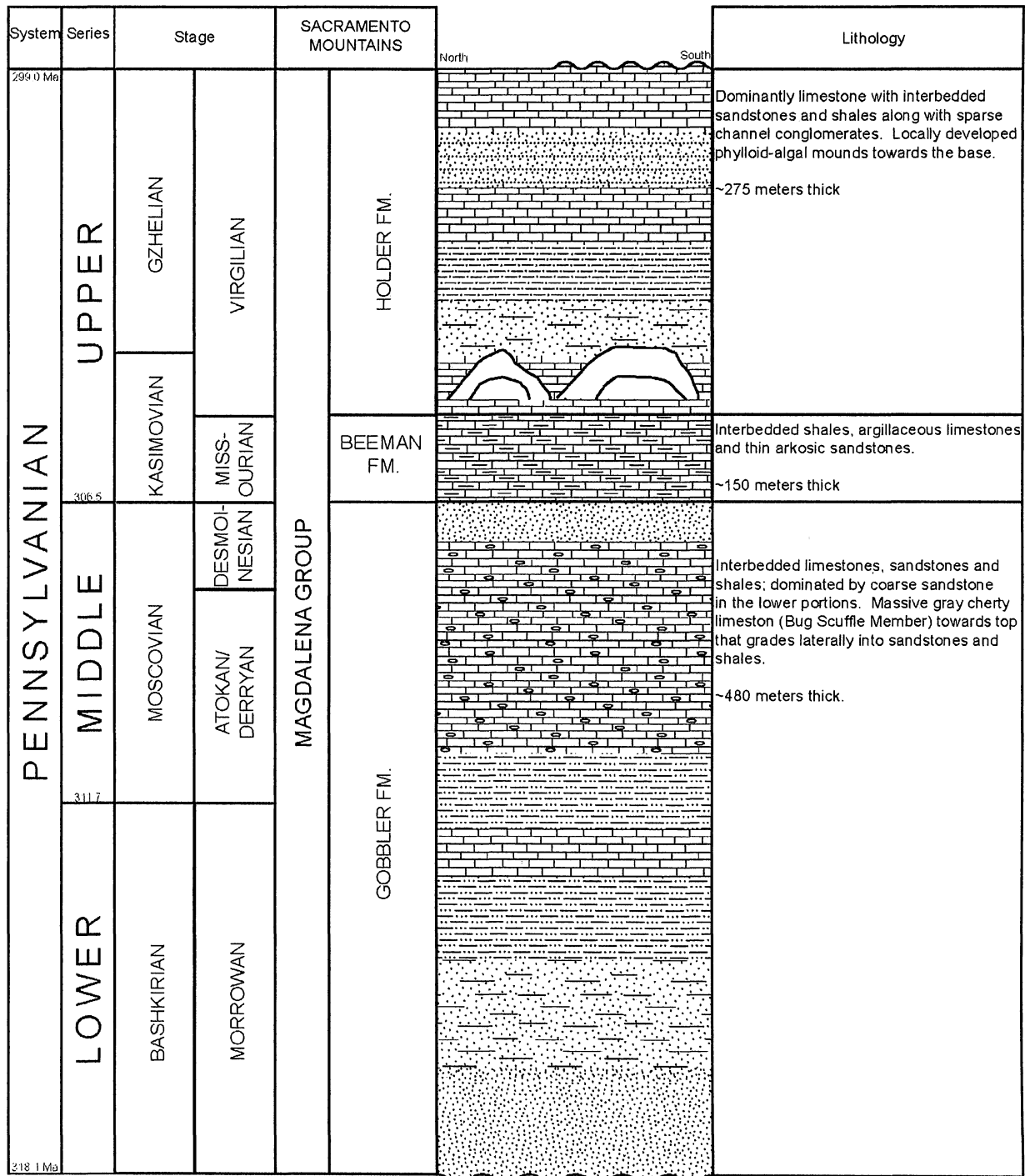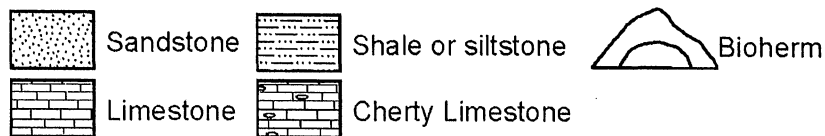~480 meters thick.

Figure 3: Generalized stratigraphy for the Sacramento Mountains displaying both ICS and North American stage names. Key to rock types below. Modified from Toomey and Babcock (1983) and Rivera (1999). Data from Pray (1961).

Sandstone Shale or siltstone Bioherm
Limestone Cherty Limestone

micrite are homogenized (Allan and Matthews, 1982), or where complex sequences of cement are identified by cathodoluminescence, but not discretely separated for chemical analysis (Goldstein, 1991).

To test the hypothesis that multiple episodes of subaerial exposure are recorded in multi-phase calcite cements, a petrographic and geochemical study of the Holder Formation was undertaken. This formation contains a series of cyclic deposits that formed during a period of Earth's history when glacioeustasy was a dominant factor controlling deposition and diagenesis of the sedimentary rocks (Heckel, 1983; Soreghan and Giles, 1999; Wilson, 1967; Goldstein, 1986). Stratigraphic studies in the Holder Formation have previously identified multiple subaerial exposure surfaces throughout the unit based on both stratigraphic (Wilson, 1967) and geochemical proxies (Goldstein, 1988a). However, geochemical studies by Allan and Matthews (1982) and Goldstein (1991), which employed whole rock or whole component data, were unable to identify the multiple episodes of meteoric diagenesis, as suggested by Wilson, (1967) and concluded that if multiple periods of exposure had occurred, meteoric waters associated with each exposure must have had similar compositions to produce nearly identical cement chemistries. This study is a re-evaluation of the diagenetic record preserved in the cements that utilizes a microsampling approach to individually analyze petrographically distinct cement phases, with the goal of delineating multiple episodes of subaerial exposure and meteoric diagenesis.

Background and Geologic Setting

Phylloid-algal bioherms are dominant features within the lower deposits of the upper Pennsylvanian Holder Formation of the Sacramento Mountains of south-central New Mexico (Figure 3). The Holder Formation was deposited on a shallow shelf in the late Pennsylvanian Orogrande Basin (Wilson, 1967) (Figure 4). The shelf extended for a short distance off the Pedernal landmass, which lay to the east, into the basin, where a series of terrigenous and carbonate sediments were deposited that make up the bulk of this formation (Wilson, 1967). During this time, there was tectonic instability in the region as the Orogrande Basin subsided along with the uplift of the Ancestral Rocky Mountains, which includes the Pedernal landmass (Soreghan, 1992; Dickinson and Lawton, 2003). Wilson (1967) characterized the lithology of the Holder Formation as two basic units: a massive and unbedded phylloid-algal mound facies dominated by mud and algae; and intermound and flanking beds of wackestones, packstones, and grainstones composed of varying amounts of skeletal material and micrite, derived largely from the mounds. The stratal geometries of the Holder Formation bioherms, which formed in response to glacioeustatic sea-level change common to the Pennsylvanian, have been intensively studied since the late 1940's, and an extensive literature has developed describing the stratigraphic relationships within the Holder Formation and correlative units (e.g. Wilson, 1967; Algeo et al., 1991; Rivera, 1999; Rankey et al., 1999; Soreghan and Giles, 1999).

In their study of Yucca Mound, Toomey et al. (1977) identified an upper and lower section of the mound, an intermound deposit consisting of a small satellite mound known as "Leopard Knob", and flanking beds. The upper mound is a phylloid-algal
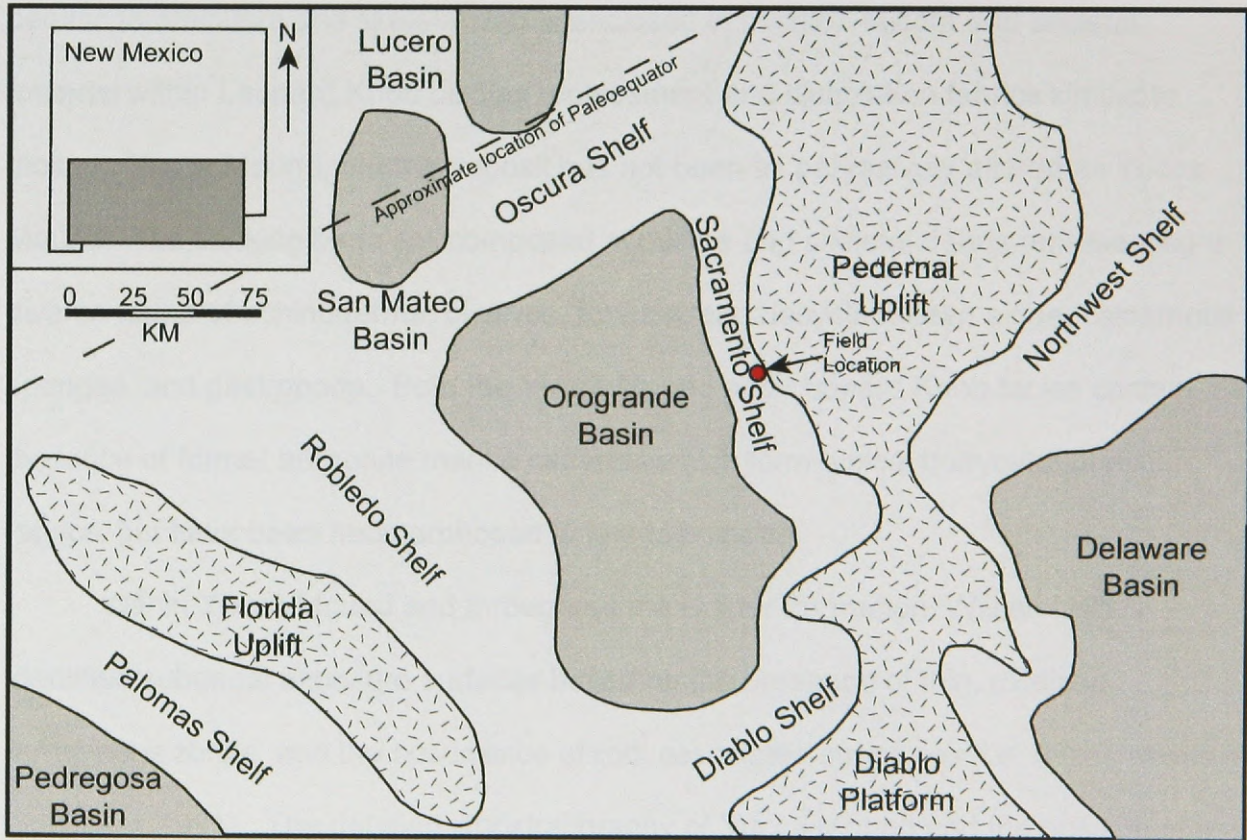
Figure 4: Paleogeographic reconstruction of the southern portion of New Mexico during the Pennsylvanian period with approximate location of field area. Modified from Algeo et al. (1991), with data from Rivera (1999) and Goldstein (1986).

9

bafflestone in which much of the micrite has been neomorphosed or removed and replaced by spar cement. Furthermore, the phylloid-algal debris has been dissolved, with the remaining voids filled by equant calcite cement. Leopard Knob is a foram-algal boundstone composed of small thrombolites of the blue-green algae *Girvanella* and benthic foraminifers and skeletal debris enclosed in micrite. Micrite and skeletal material within Leopard Knob display replacement and dissolution fabrics similar to those in Yucca Mound, but the deposit has not been as pervasively altered as Yucca Mound. The flanking beds are composed of micrite and skeletal debris representing a diverse fauna of echinoderms, bivalves, foraminifers, dasycladacean algae, calcareous sponges, and gastropods. Both the Yucca Mound and Leopard Knob facies contain evidence of former aragonite marine cements which form typical botryoidal growth fabrics, but have been neomorphosed to low-Mg calcite.

Within Yucca Mound and throughout the Holder Formation, Wilson (1967) identified subaerial exposure surfaces based on the presence of thin, oxidized ferruginous zones, and the occurrence of root associated structures (i.e. rhizocretions of Goldstein, 1991). The detailed lithostratigraphy of Yucca Mound and the position of the surfaces of exposure are illustrated in Figure 5. Based on the petrographic character and lateral extent of cathodoluminescent calcite cements associated with these exposure surfaces, Goldstein (1986, 1988b) constructed a general cement stratigraphy for the Holder Formation. He identified an early cement associated with meteoric phreatic diagenesis, and late cements formed during burial from warmer, subsurface brines rich in Fe. During his analysis of Yucca Mound, he found the early cement to be the dominant phase occluding the porosity within the mound with a minor amount of the
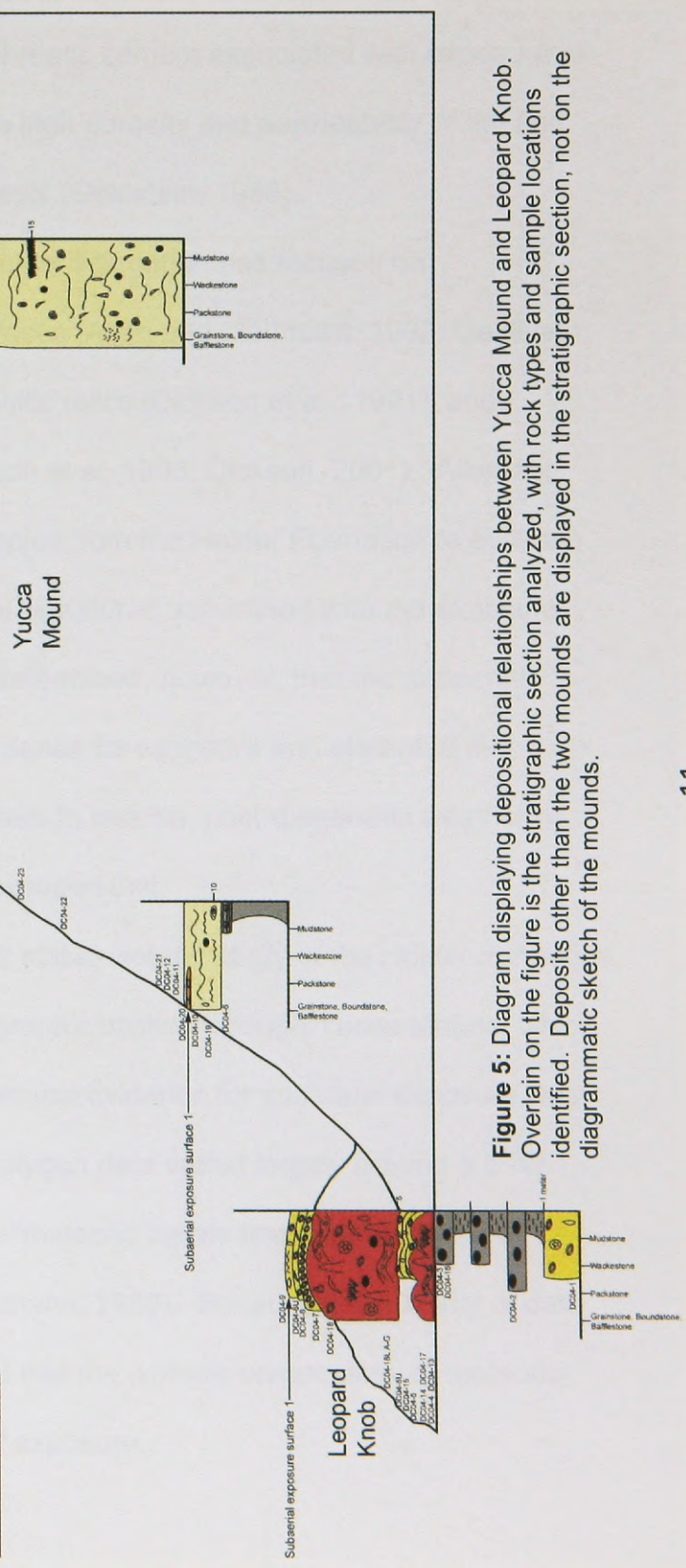
Figure 5: Diagram displaying depositional relationships between Yucca Mound and Leopard Knob. Overlain on the figure is the stratigraphic section analyzed, with rock types and sample locations identified. Deposits other than the two mounds are displayed in the stratigraphic section, not on the diagrammatic sketch of the mounds.

11

late burial cement present near the top of the mound. He concluded that the mound was occluded by a single phase of early, phreatic cement associated with exposure at the top of the mound, which was due to the high porosity and permeability of the unit during the early stages of meteoric diagenesis (Goldstein, 1986).

Prior geochemical analysis of the Holder Formation has focused on characterization of subaerial exposure surfaces (Allan and Matthews, 1982; Goldstein, 1988a, 1991), analysis of preserved aragonitic relics (Dickson et al., 1991), and biogenic components within the unit (Dickson et al, 1996; Dickson, 2001). Allan and Matthews (1982) analyzed whole rock samples from the Holder Formation to evaluate the development of distinctive geochemical signatures associated with the exposure surfaces defined by Wilson (1967). They determined, however, that the subaerial exposure surfaces lacked geochemical evidence for exposure and attributed this apparent lack of distinct geochemical markers to intense, post-diagenetic weathering which removed the top few meters of the exposed unit.

Goldstein (1991) undertook a similar stable isotope study in the Holder Formation focused on paleosol carbonates in a stratigraphic section through Yucca Mound, which contained two exposure surfaces. Geochemical evidence for subaerial exposure was present at only one surface. Carbon and oxygen data varied largely around a $\delta^{18}O$ value of -5.5‰ which he interpreted as the "meteoric calcite line" characteristic of carbonate altered by meteoric waters (Lohmann, 1988). Because the majority of data converged toward this value, he suggested that the isotopic composition of meteoric waters was similar during both episodes of exposure.

12

CHARACTERISTICS OF LITHOLOGIC UNITS

Petrology and Petrography

This study of Yucca Mound and Leopard Knob is based on detailed petrographic and chemical analysis of the lithologies comprising those deposits, and that of the flanking beds overlying the mounds. Lithologic descriptions were performed on polished slabs, with analysis of microfabric and cement relations performed using transmitted light and cathodoluminescence petrography of 50 thin sections.

Yucca Mound

The dominant lithology present throughout Yucca Mound is a phylloid-algal bafflestone (Figure 6) composed of highly fragmented and replaced plates of the phylloid-algae *Eugonophyllum* (Konishi and Wray, 1961; Toomey and Babcock, 1983). The original skeletal carbonate of the phylloid-algae is usually absent due to dissolution, with these moldic pores largely occluded by equant calcite cement prior to burial and compaction. The rock matrix is composed of micrite that contains ostracods and small benthic foraminifera, with fragments of brachiopods, crinoids, and bivalves. This micrite typically shows evidence of neomorphism to microspar, but also contains large vugs occluded by large (up to 3 mm) equant calcite cement. Furthermore, skeletal material has also been highly altered and is replaced by low-Mg calcite. Foram-algal packstones are also present toward the top of the mound which display neomorphic fabrics similar to the bafflestone but contain about 10% less algae and considerably more (10-15%) small benthic and encrusting foraminifera (Figure 9). All porosity is similarly occluded by large, equant calcite cement.
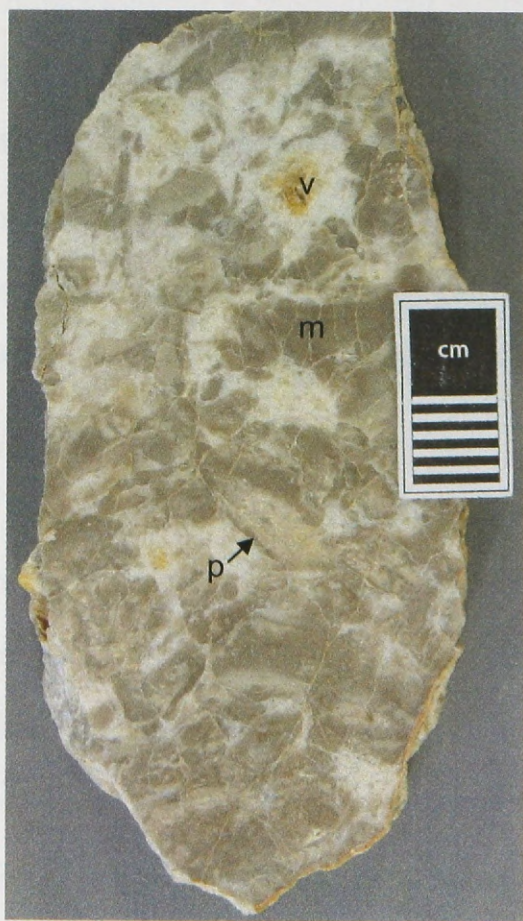
Figure 6: Outcrop (A) and hand sample (B) photographs of phylloid-algal mound material. A. Note layered appearance of rock in outcrop. These layers are the cement filled remains of the phylloid-algae (p) *Eugonophyllum*. Tan to gray material are clumps of micrite. Core hole in rock is about 2.5 cm in diameter. B. The polished surface of the rock shows clumps of micrite (m), and thin, cement filled phylloid-algae (p). Note the large vugs (v) that contain cement.

Leopard Knob

Leopard Knob is composed of a rock type termed "leopard rock" (Toomey et al., 1977, Toomey and Babcock, 1983), which displays a distinctive blotchy fabric formed by black microbial thrombolitic structures interspersed with coarse spar that weathers light tan or yellow due to limonite staining (Figure 7). The thrombolites appear as plumose or digitate structures that are composed of tubular, encrusting foraminifera that are coated with fine tubules of the blue-green algae *Girvanella*. The micrite matrix enclosing the thrombolitic boundstones contains abundant skeletal debris that includes bivalve, ostracod, and phylloid-algae fragments, as well as dasycladacean algae of the genus *Macroporella*. This rock can be described as a foram-algal/microbial boundstone. Primary porosity is isopachously rimmed by prismatic calcite cement which is overlain by large (up to 5 mm in diameter) equant calcite cement. As observed above in Yucca Mound, most of the micrite has been neomorphosed to microspar that displays cathodoluminescence characteristics similar to calcite cements filling adjacent porosity, and skeletal debris has been largely replaced by low-Mg calcite cement (Figure 9). Minor silicification is commonly present within the microspar that replaces micrite.

Flanking Beds

The flanking beds, which drape Yucca Mound and Leopard Knob, comprise fossiliferous wackestones and grainstones, along with sparsely fossiliferous mudstones and thin interbedded shales (Figure 8). All the porosity within the grainstones has been occluded by equant calcite cement. Fossiliferous units contain debris derived from the mound such as phylloid-algal fragments, bivalve and ostracod debris, small benthic and encrusting foraminifera, sparse brachiopod shells, echinoderm debris, and fusulinids.
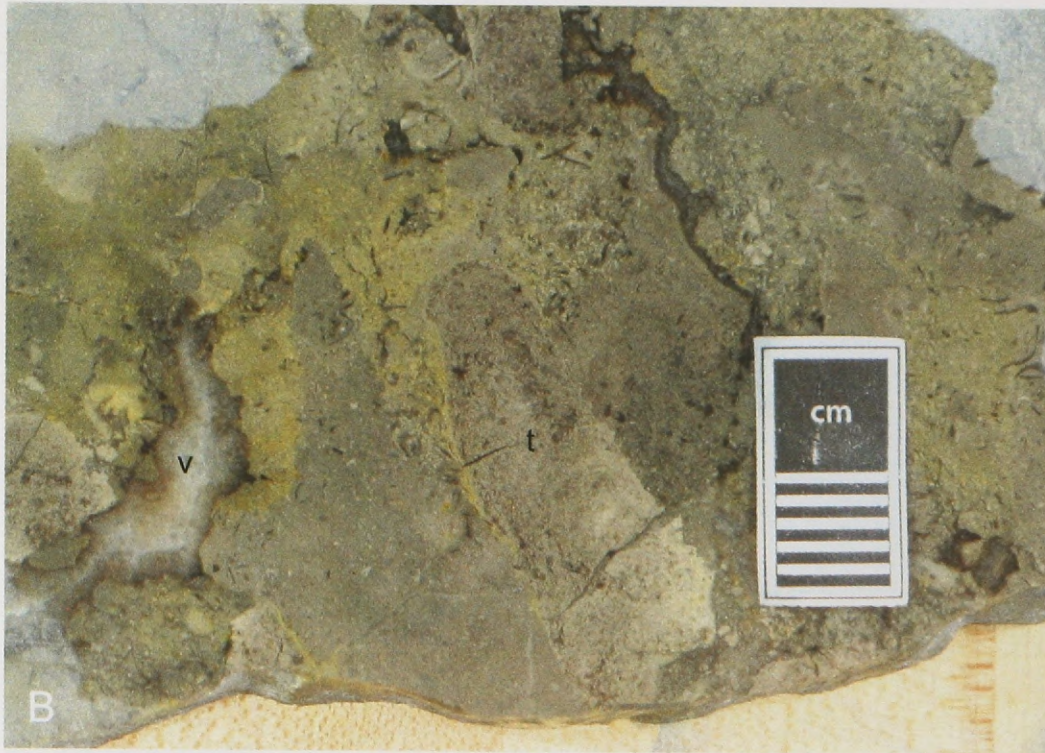
Figure 7: Outcrop (A) and hand sample (B) photographs of the leopard rock foram-algal/microbial boundstone facies. A. Outcrop photo displaying the characteristic weathering profile common in leopard rock, where *Girvanella* and foraminifera dominated thrombolites weather black, while cement weathers a light tan. Pen for scale is 13 cm long. B. Polished hand sample displaying thrombolites (t) and large vug (v) filled by calcite cement.

16

Figure 8: Outcrop photographs of flanking beds that overlie the mounds. A. Interbedded grainstones, mudstones, wackestones, and shale that make up the flanking beds overlying Leopard Knob. Hammer is ~25 cm in height. B. Wackestone facies overlying the lower leopard rock facies. Note typical thickening and thinning character developed in the beds overlying the irregular mound surface. Backpack is ~1/3 meter tall.

In micritic lithologies, local areas contain abundant identifiable peloids, whereas the bulk of the micrite has been neomorphosed to microspar or locally dissolved to produce large voids filled with equant calcite, with cement features similar to those observed in the mound lithologies (Figure 9).

<u>Subaerial Exposure Horizons</u>

Within the mounds and flanking beds, two subaerial exposure horizons were identified (Figure 5). One developed in the upper few meters of Yucca Mound, and the other, that is highly dolomitized, is present in the overlying flanking beds. These horizons display reddish or orange staining due to oxidation of iron, intense dolomitization, and commonly possess pedogenic features such as rhizoconcretions (Wilson, 1967; Goldstein, 1986, 1991).

Figure 9: Thin section photomicrographs of the characteristic lithologies in Yucca Mound (A and B), Leopard Knob (C and D), and flanking beds (E and F). A and B. Phylloid-algal bafflestones that make up most of Yucca Mound. Note that phylloid-algal (p) aragonite has been dissolved and replaced by calcite spar. In B, note fossiliferous micrite filling inter-algal spaces. C. Foram-algal/microbial boundstone from Leopard Knob displaying a contact between thrombolites (t) and the micritic (m) matrix. D. Contact in leopard rock facies showing vuggy (v) dissolution void in the micritic (m) matrix. E and F. Grainstone (E) and packstone (F) flank bed facies consisting of mound-derived small benthic foraminifera (f) and phylloid-algae (p) debris. Scale bars are 500 μm in length.
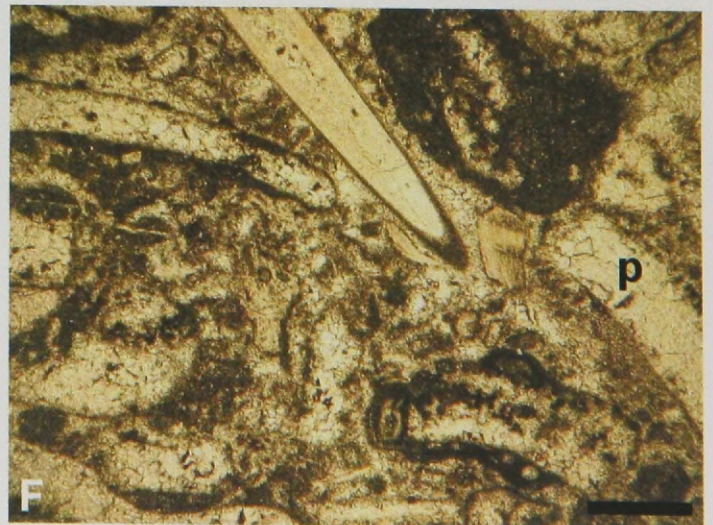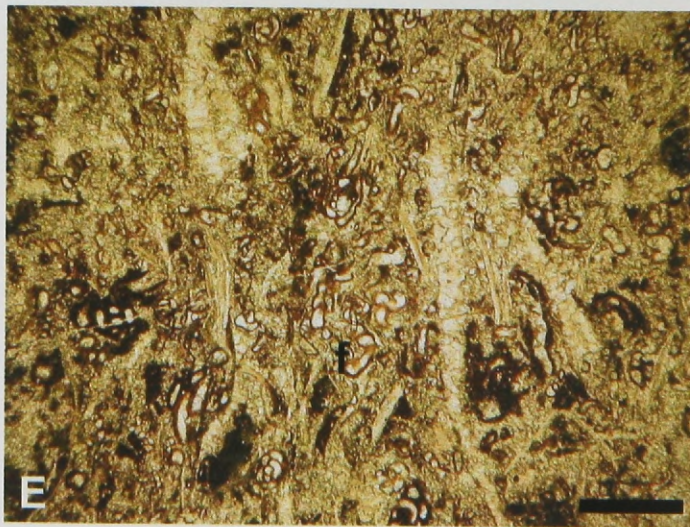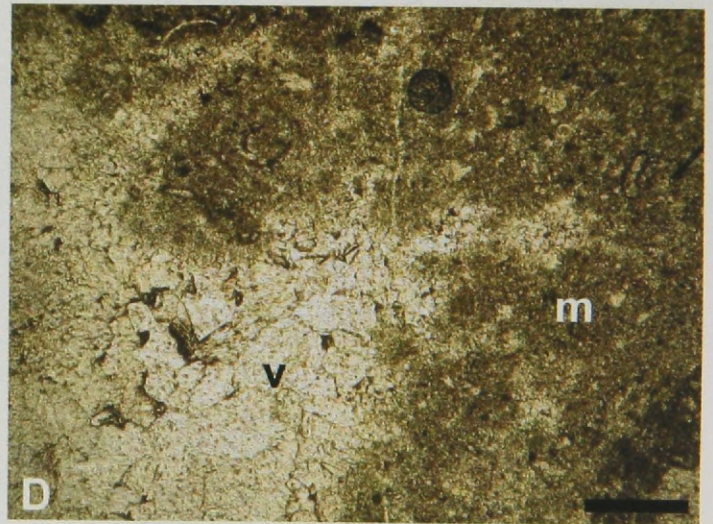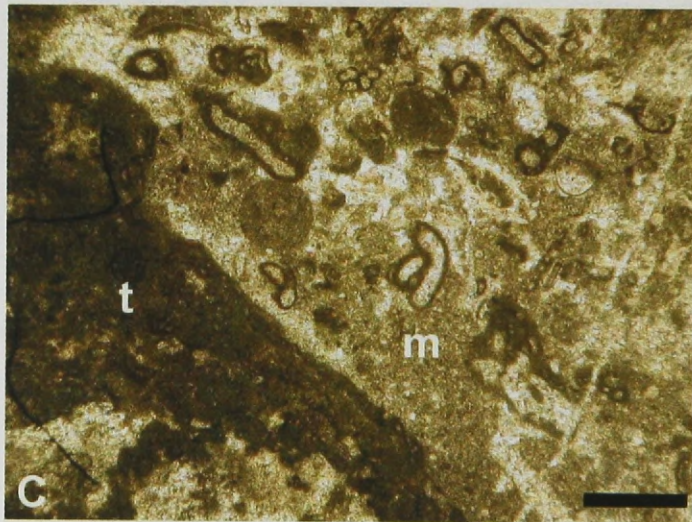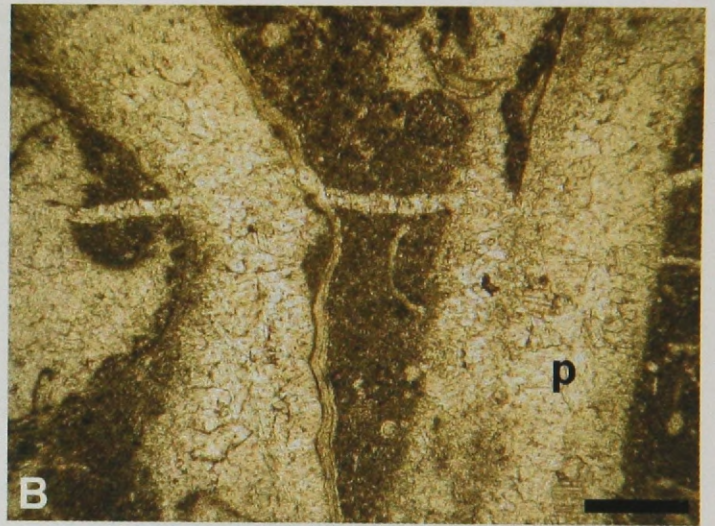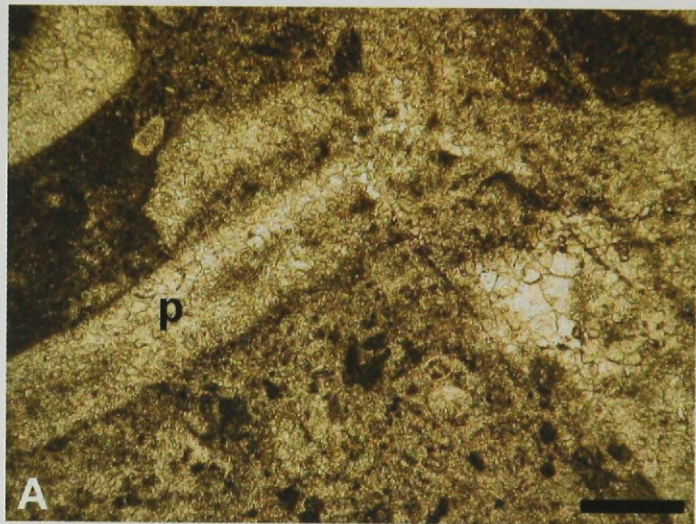
THE CEMENT RECORD OF DIAGENESIS

Calcite cement is present throughout the sequence in mound and flanking bed facies in a combination of primary and secondary pores. Though present, primary porosity, developed as shelter voids and inter- and intra-granular pores in grainstone facies, is comparatively small and volumetrically minor relative to secondary porosity formed through dissolution of allochems and vuggy porosity within micritic facies. Given the abundance of original aragonite mineralogies of many of the allochems, such as plates of phylloid-algae, secondary moldic porosity (Choquette and Pray, 1970; Longman, 1980; Kirkland et al., 1993) is a significant contributor to the porosity network subsequently occluded by equant cements. However, it is notable that the micritic matrix which has undergone extensive neomorphism also exhibits local areas of dissolution, with the development of large solution vugs which dominate as areas in which equant calcite cements are developed. It is within this porosity network that the record of the sequence of calcite cements precipitated can be best documented and the geochemical character of discrete cement phases can be obtained.

Multiple phases of cement were identified through petrographic observation including the evaluation of crystal growth fabrics with transmitted and polarized microscopy, and cathodoluminescence (CL) techniques to discriminate the growth sequence and the nature of contacts between successive stages of cementation. Differences are apparent between cement sequences occurring in primary porosity and pores developed by secondary dissolution. Primary pores are typically lined with isopachous fringes of fine prismatic calcite (Figure 10), which in turn are overlain by calcite with either concordant contacts or with evidence of partial corrosion. Based on
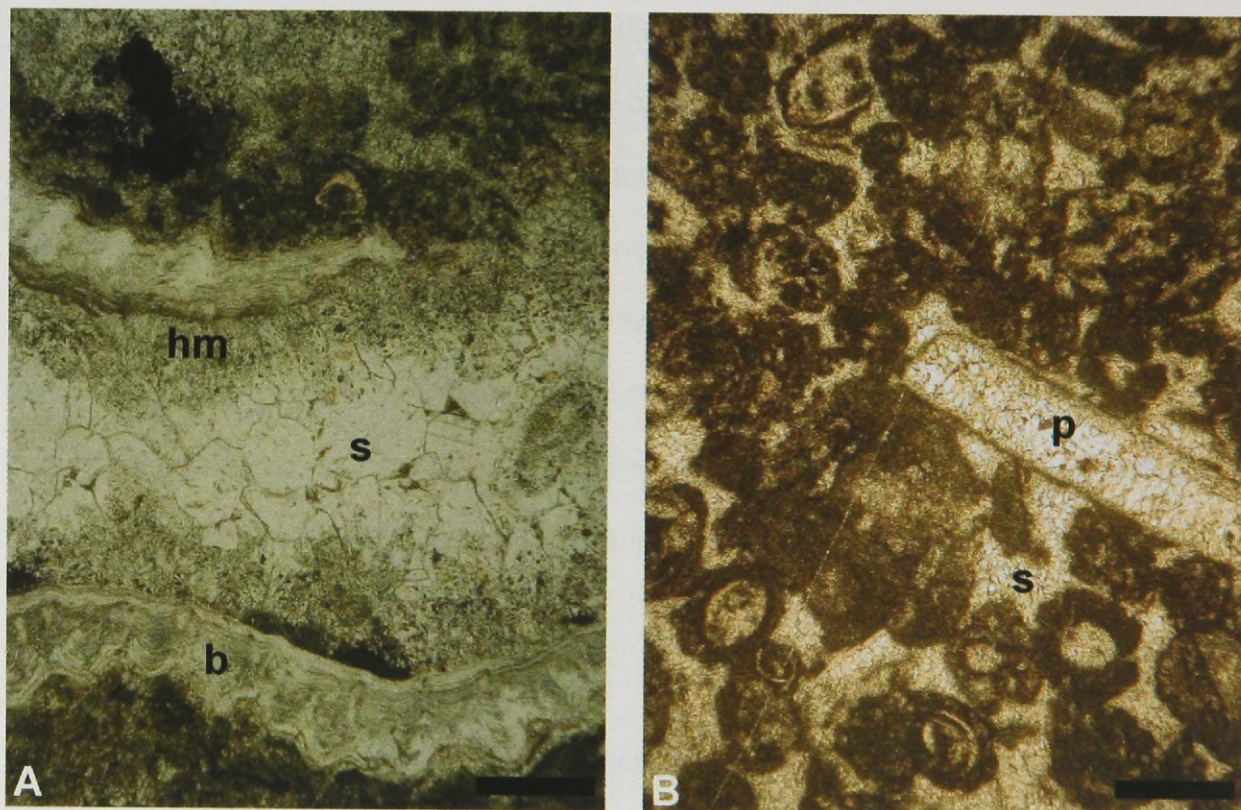
Figure 10: A. Intraparticle porosity in a brachiopod shell (b) from a flanking bed overlying Leopard Knob. Note mottled prismatic cement (hm) lining the edges of the pore. The remaining clear, equant calcite cement (s) is the dominant cement in the unit. B. Interparticle porosity in a grainstone overlying Leopard Knob occluded by equant spar (s). Moldic porosity occurs within phylloid-algal (p) debris, and has been occluded by low-Mg calcite spar. Scale bars are 500 μm in length.

CL and geochemical characteristics, the calcite cements have been subdivided into five distinct phases of cement growth, termed here as Cements I through V (Figure 11).

Cement I

This cement comprises an early isopachous prismatic calcite that grades into a late equant calcite that are both commonly the first cements precipitated in primary porosity or secondary porosity and are only observed below the first exposure surface. Early Cement I is highly mottled under CL and contains abundant inclusions. It then grades into late Cement I, which is a CL zoned calcite with thin (<5 μm), alternating non- and dully luminescent bands (Figure 11A, B, & D). The phase is volumetrically minor when present as compared to the other cements. Furthermore, late Cement I is commonly nucleated on early Cement I, which is interpreted as recrystallized high-Mg marine cement (James and Choquette, 1990a; Land, 1970; Lohmann and Meyers, 1977).

Cement II

This cement is a zoned, dully luminescent calcite that is the first cement precipitated on rims of pores when Cement I is absent. Cement II is restricted stratigraphically to 10 meters or more below the second exposure surface and occurs primarily in secondary porosity (Figure 11C & D). This phase of cementation is volumetrically minor, as is Cement I. When Cement I is present, Cement II is precipitated epitaxially with a sharp, non-corrosive contact between these phases. Cement II commonly exhibits a scalenohedral crystal fabric, with rhombic to acute terminations. Cement II, in turn, is overlain by Cement III with very little to no corrosion observed at the contact.

Cement III

Cement III is non-luminescent and consists of scalenohedral to rhombohedral crystals (Figure 11B, C, D, E, & F). When not preceded by Cement I or Cement II this cement is the initial cement occluding porosity and comprises both prismatic and equant crystal fabrics. When preceded by Cement I or II, the crystals of Cement III are much larger than the previous cements and make up the first phase extending into equant cements. Volumetrically, the phase occludes between 20-80% of the porosity. When this cement is overlain by Cement IV, the contact is sharp, with no evidence of corrosion. When Cement IV is absent, this cement is overlain by Cement V and displays evidence of corrosion. In many places, small fractures crosscut Cement III and these are occluded by Cement V (Figure 19).

Cement IV

Under CL, Cement IV is a brightly luminescent equant calcite that is zoned with thin (<20 µm thick) non-luminescent or moderate luminescent bands (Figure 11B, C, D, E, & F). When this cement is present, it forms epitaxially on Cement III with a scalenohedral crystal fabric, and can occlude up to 50% of porosity. When Cement IV is present, while the contact with underlying Cement III is concordant, the contact with overlying Cement V is highly corroded, sometimes to an extent that Cement IV is present only as a thin band that lines the edges of Cement III.

Cement V

Cement V, the final cement phase that occludes all remaining porosity, is a massive, dully luminescent equant calcite that appears highly mottled with small areas of moderate luminescence (Figure 11C, D, E, & F). This cement is locally absent, but

where present can occlude up to 80% of the porosity. Significantly, fractures developed

in previous phases of cement are always filled by Cement V.

Figure 11: Cathodoluminescence (CL) photomicrographs of calcite cements displaying variable luminescence, and growth forms. Scale bars are 500 μm in length. A. CL photomicrograph of Figure 10, Part A; sample DC04-8U. Cement I (C1) fills primary porosity in a brachiopod shell. Note the multiple, thin (less than 5μm) dully and non-luminescent zones common to this cement. It appears as if two separate stages of growth for this cement phase occluded this pore, the first being the mottled prismatic cement rimming the pore, early Cement I (hm), and second the zoned late Cement I growth. B. Cement I (C1), Cement III (C3), and Cement IV (C4) occluding porosity, and showing the highly zoned nature of Cements I and IV; sample DC04-18. Note corroded surfaces (c) of Cement IV and the typical amounts of pore space filled by each cement phase. C. Secondary porosity occluded by Cement II (C2) precipitated directly on the substrate (s), followed by Cement III (C3), Cement IV (C4), and Cement V (C5); sample DC04-18L-B. Cement IV was precipitated epitaxially to Cement III, and then partial dissolution (c) occurred prior to Cement V precipitation. Also, note typical scalenohedral and rhombic terminations of Cement II, the zoning characteristic of cement IV, and the mottled, unzoned fabric of cement V. D. Primary pore within a brachiopod shell occluded by a complete sequence of cement phases (C1, C2, C3, C4, and C5); sample DC04-20. Cement IV has been almost completely dissolved, and only a thin brightly luminescent remnant lines the edges of Cement III. Cement I appears as if there has been at least three separate stages of growth displaying the same distinct luminescence zones (dull, non, and bright). E. Cement III (C3) precipitating directly off the substrate (s); note typical scalenohedral crystal form of Cement IV (C4) and dull-luminescence of Cement V (C5); sample DC04-27. F. Cements in moldic pore from dissolution of aragonitic phylloid-algae; sample DC04-33. Samples E and F lack Cement I and II because they occur above (are younger than) the first subaerial exposure surface (Figure 5).
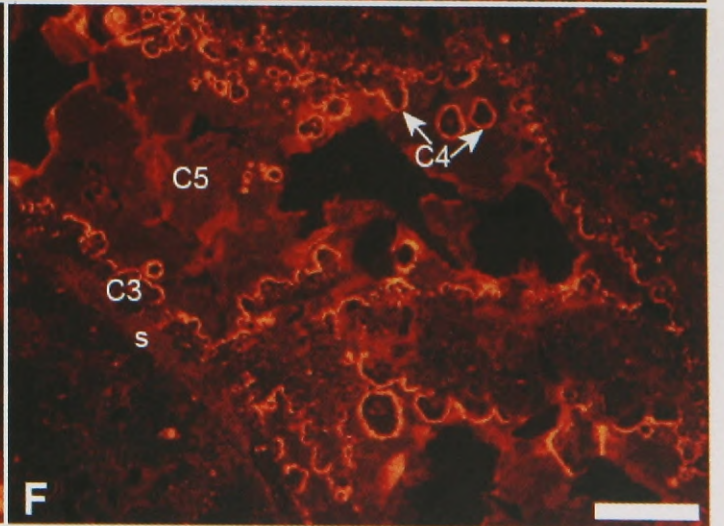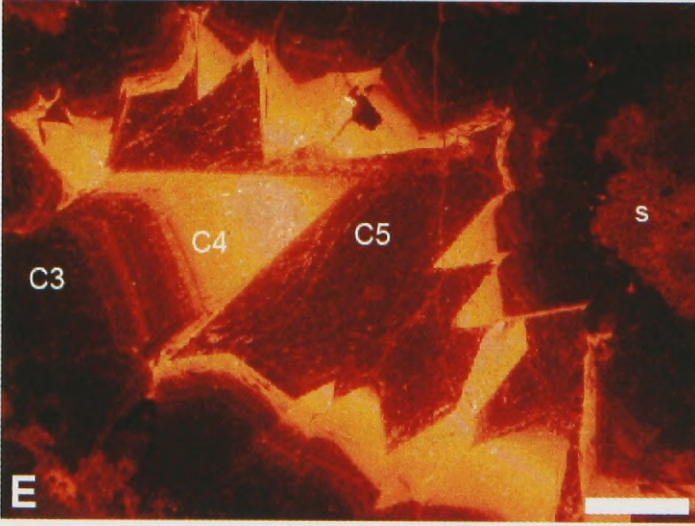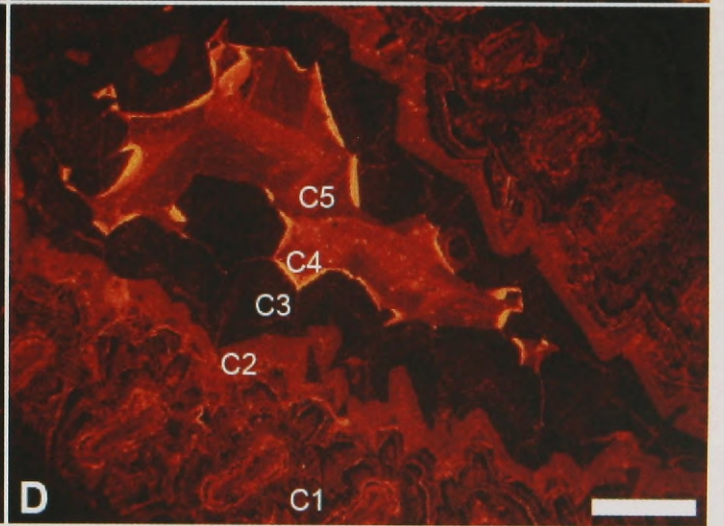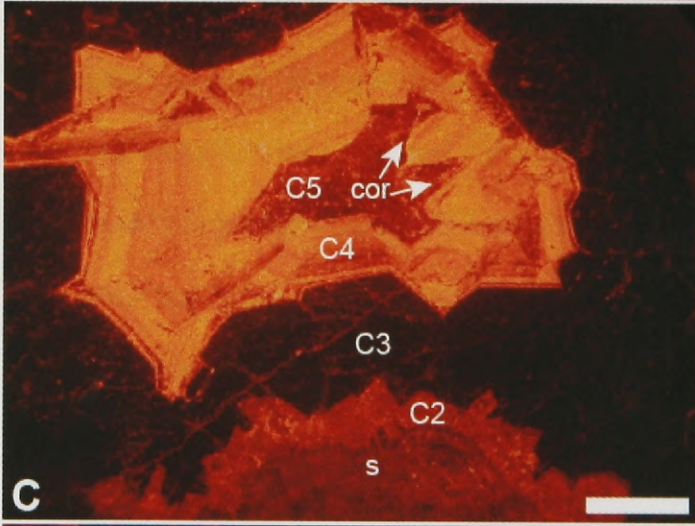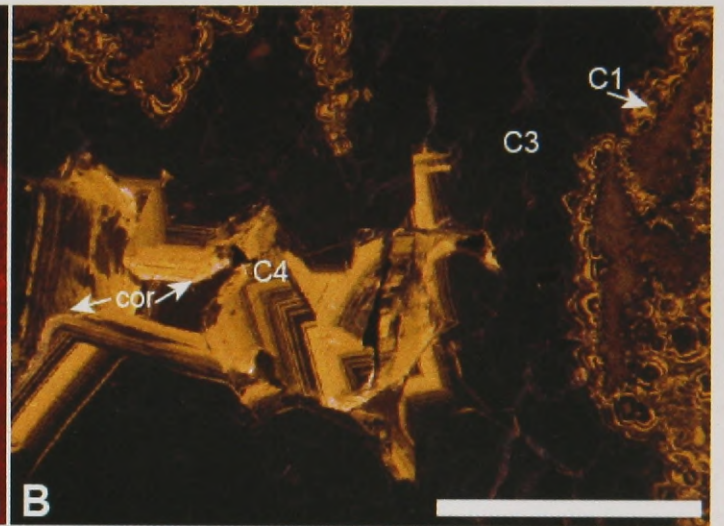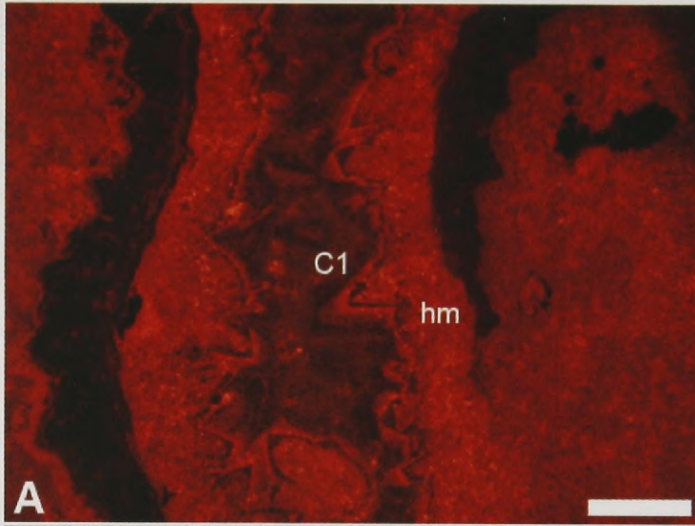
GEOCHEMICAL CHARACTERISTICS OF CEMENT PHASES

Carbon and Oxygen Isotopic Chemistry

Each individual cement phase was microsampled following the procedure of Benito et al. (2001) to retrieve a minimum of 20 µg of material. These microsamples were then roasted at 200°C in vacuo for one hour to remove volatile organic matter and water. Samples were placed in individual reaction vessels and reacted at 76° ± 2°C with anhydrous phosphoric acid in a Finnigan MAT Kiel preparation device coupled directly to the inlet of a Finnigan MAT 251 triple collector isotope ratio mass spectrometer. Oxygen isotope ratios were adjusted for O^{17} contribution (Craig, 1957), and were further corrected for acid fractionation and source mixing by calibration to a best-fit regression line defined by two NBS standards, NBS-18 and NBS-19. Data are reported in per mil (‰) notation relative to VPDB. Precision and accuracy of data were monitored through daily analyses of a variety of powdered carbonate standards. Measured precision was maintained at better than 0.1‰ for both carbon and oxygen isotope compositions.

Cement I defines a field centered on -4.8‰ $\delta^{18}O$, with a range in $\delta^{13}C$ from -0.4 to 1.6‰ (Figure 12). The observed range in $\delta^{18}O$ (-4.2 to -7.3‰) can be seen in figures 12 and 17. While $\delta^{18}O$ values remain consistent throughout the section, $\delta^{13}C$ values steadily increase stratigraphically down-section (Figure 13). Most Cement I samples are taken from areas where primary porosity is present, and recrystallization of marine cement is evident (Lohmann and Meyers, 1977).

Cement II defines a field of values centered at -5.5‰ $\delta^{18}O$ with $\delta^{13}C$ varying from -0.8 to 3.0‰ (Figure 12). Carbon values increase down-section, with the most positive values derived from Cement II samples precipitated in Leopard Knob (Figure 13).

The $\delta^{18}O$ values of Cement III are slightly more negative than those of Cement II and define a field with an average of -5.6‰ (Figure 12). Cements II and III are similar isotopically to cements analyzed by both Goldstein (1991) and Fernberg (1987) whose values define a field with an average of -5.5‰ $\delta^{18}O$, which was designated by Goldstein (1991) as the meteoric calcite line for the entire unit. Cement III displays both the most negative and positive carbon values, ranging from -1.6 to +5.2‰ $\delta^{13}C$, with the most positive $\delta^{13}C$ occurring in the lowermost part of the section (Figure 13).

Cement IV displays more negative $\delta^{18}O$ values than the previous cements with an average value of -6.3‰ and with a small range in $\delta^{13}C$ from -0.5 to +1.2‰ (Figure 12). Not only is the average $\delta^{18}O$ more negative than the previous cements, but the values display greater variation, ranging from -5.9 to -6.7‰. In contrast to all previous cements, the $\delta^{13}C$ values of Cement IV exhibit a decrease in variability down section and become more negative (Figure 13).

The $\delta^{18}O$ values of Cement V exhibit the greatest variation, ranging from -6.5 to -8.6‰, and most negative average value of -7.3‰. Values for $\delta^{13}C$ are always positive, but are also highly variable, ranging from +0.1 to +2.6 with no apparent stratigraphic trend (Figure 12).
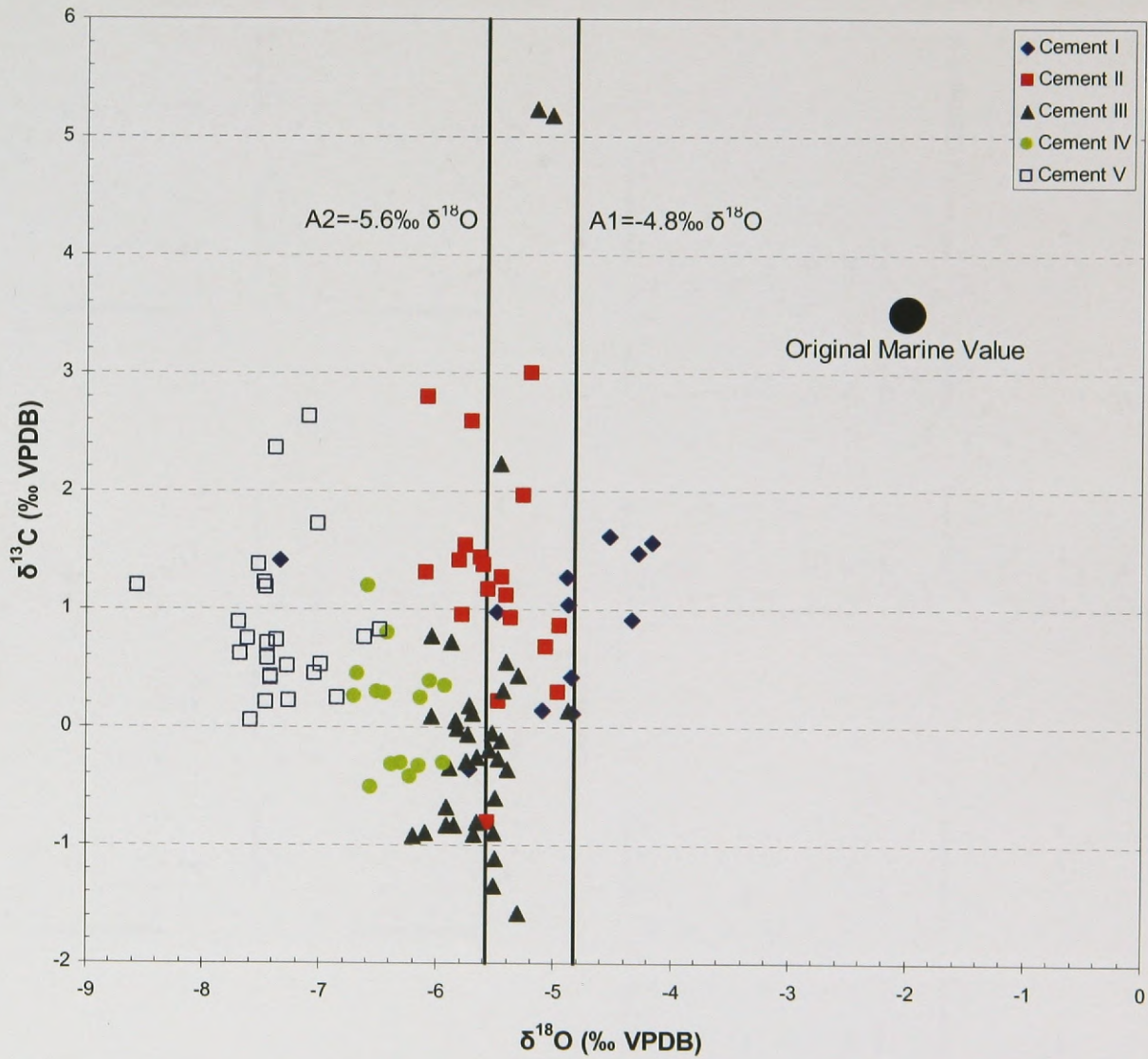
Figure 12: Carbon and oxygen isotopic composition of calcite cement phases. A1 and A2 refer to the average $\delta^{18}O$ values for meteoric diagenesis stage one and stage two respectively. An original marine value of -2‰ $\delta^{18}O$ and 3.5‰ $\delta^{13}C$ for marine precipitates is plotted for reference (Lohmann and Walker, 1989; Veizer, 1999; Mii et al., 1999).

Figure 13: Carbon and oxygen isotopic composition, with trace element ratios of each cement phase as compared to stratigraphic position, determined from figure 5.
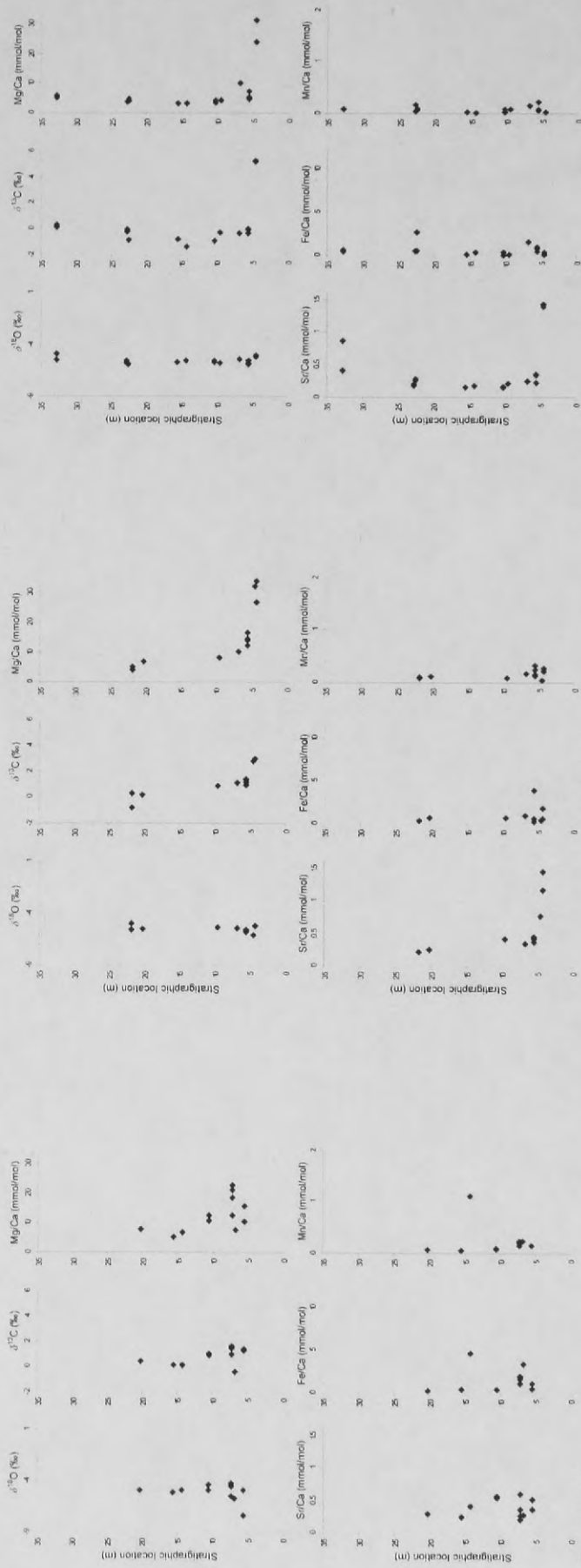
Cement I

Cement II

Cement III
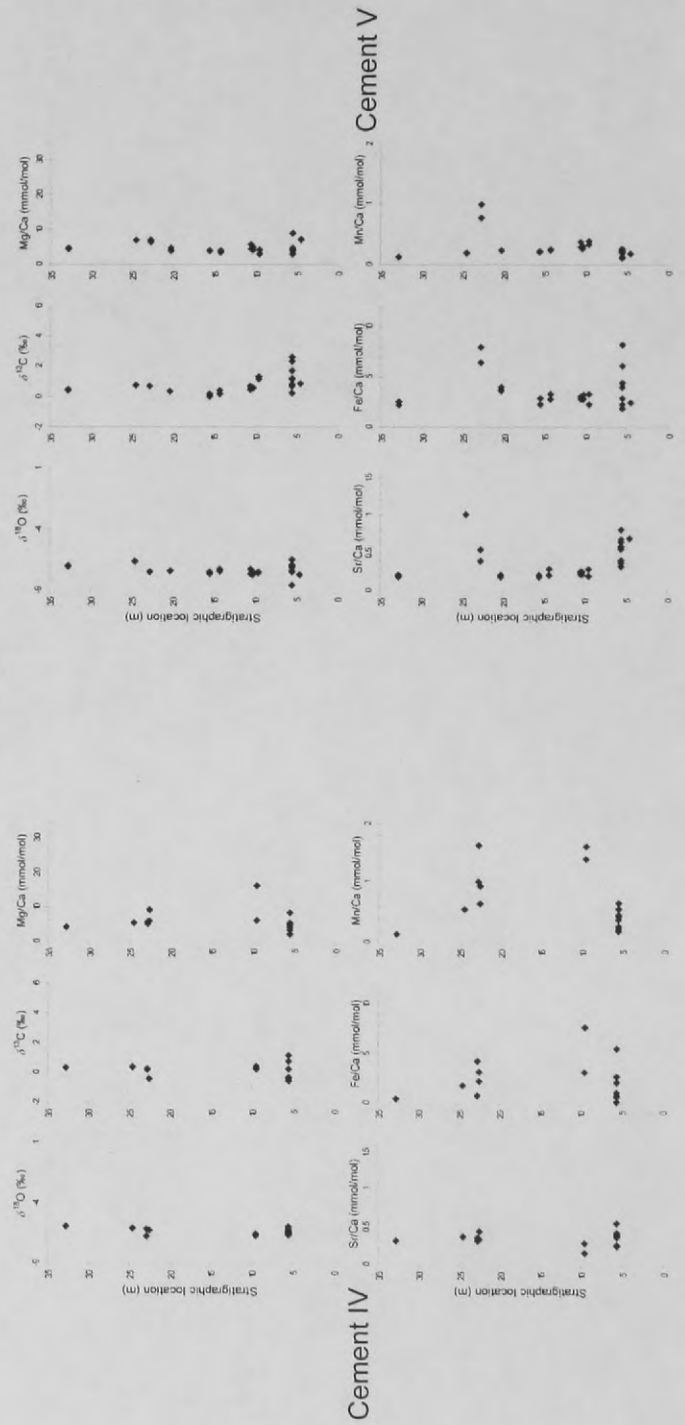
Cement IV

Cement V

Minor Element Chemistry

Two separate determinations of minor elemental contents were undertaken in this study: electron microbeam analysis (EMPA) of multi-phase calcite cement and inductively coupled plasma mass spectrometry (ICP-MS) measurements of powdered cement material. Electron microbeam analysis was performed on an SX-100 Cameca Microprobe to measure elemental quantities of Ca, Mg, Sr, Fe and Mn within the multiple phases of calcite cement delineated through cathodoluminescence microscopy. All analyses were conducted with an accelerating voltage of 15 kV, intensity of 10 nA, and a spot size of 10 μm. Detection limits were 750 ppm for Ca, 150 ppm for Mg, 600 ppm for Fe, 550 ppm for Mn, and 1000 ppm for Sr. Splits of the powdered samples used for isotopic analysis were taken and a second determination of elemental content was conducted utilizing inductively coupled plasma-mass spectrometry (ICP-MS) techniques. The samples were first dissolved in 1.2 mL of dilute Fisher Optima grade 1% HNO_3 + 2% HCl spiked with indium as an internal standard. The samples were further diluted with 1% HNO_3 solution spiked with indium as a final preparation before analysis. Sample solutions were then analyzed on a Finnigan *Element* ICP-MS. Run precision was better than 0.5% for Mg/Ca and Sr/Ca while Fe/Ca and Mn/Ca ratios had precision better than 2%, based on the relative standard deviation determined from multiple analyses of a laboratory standard. Comparison of elemental ratios determined with EMPA and ICP-MS were within a factor of ten with the exception of a few outliers, which have been attributed to unresolved machine and/or operator errors (e.g. sample size below detection for ICP-MS; insufficient polish on samples for microbeam analysis;

or inaccurate microdrilling of phases). All data are reported here as minor element to calcium ratios (mE/Ca) as millimole/mole (mmol/mol) ratios.

Cement I has an average Mg/Ca ratio of 12.7, ranging from 5.22 to 22.8. An average Sr/Ca value of 0.396 is comparable among all cement phases and exhibits a narrow range of values from 0.215 to 0.611 (Figure 14). Fe/Ca and Mn/Ca values are consistently low with averages at 1.51 and 0.237 respectively, with Fe/Ca never exceeding 5.0 and Mn/Ca always below 0.3 (Figure 15). Stratigraphically, the highest Mg/Ca values for Cement I are observed within Leopard Knob, while the lowest values are in the upper part of the section in Yucca Mound (Figure 13). Sr, Fe, and Mn display no stratigraphic trends.

Cement II has a slightly higher Mg/Ca ratio than Cement I, with an average of 14.9 and a larger range, from 4.18 to 33.7. The Sr/Ca average is 0.525, which is slightly greater than Cement I, and displays a range from 0.180 to 1.45 (Figure 14). Fe/Ca and Mn/Ca ratios of Cement II are also low, averaging 0.883 and 0.146 respectively but with a similar range to Cement I (Figure 15). The Mg/Ca ratio exhibits considerable stratigraphic variation, with Leopard Knob and the lower part of the section displaying the highest values, and the upper part of Yucca Mound having the lowest values (Figure 13).

Cement III has an average Mg/Ca ratio of 6.22 which is lower than that of Cements I and II, and displays a broad range in values from 3.09 to 31.2 (Figure 14). The Sr/Ca ratio is similar to Cement II, but Fe/Ca and Mn/Ca averages are lower at 0.553 and 0.0833 respectively (Figure 15), and Fe/Ca and Mn/Ca do not exceed 3.0 and 0.2 respectively. Both Mg/Ca and Sr/Ca vary stratigraphically, with the highest
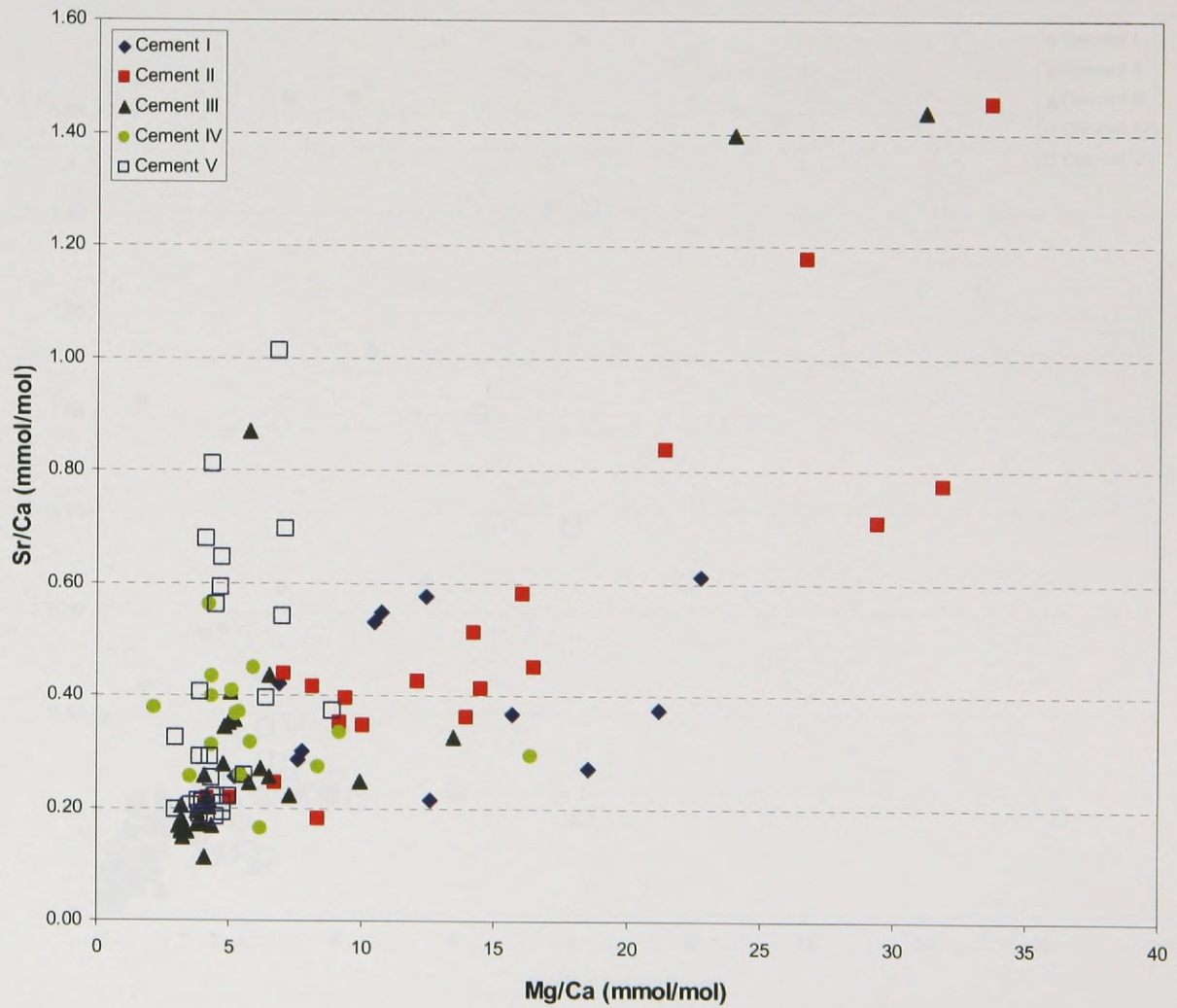
Figure 14: Minor element ratios comparing Sr/Ca to Mg/Ca for the calcite cement phases.

ratios resulting in the lower part of the diagram and the highest ratios correlated to the uppermost [figure 15].

Cement IV forms the strongest variability observed in Cements I-II and in Mg/Ca ratios at 2... system level 0.13 and 0.42 (0.33 average) the Mn/Ca (0.06 and 0.85) plots 15c and Fe/Ca average 0.81 ranging from 0.04 Fe to ... Mn/Ca is greater than Cements I, II, and III with an average value of 0.074 which ...

... decrease in the cement (Mucci, 1988).

... The Mn/Ca value of Cement V has the lowest average of all cements and ... 0.19 and a Fe/Ca range of ... to ... the average value of 0.242 for Cement V ...

... in Cement IV but has its own variability from 0.10 to 0.19. Cement ... less Fe than Cement II. The average Fe/Ca value of 3.0 ... and a range from 1.6 ... to 16.1. The average Mn/Ca value is 0.275 which is less than Cement II, but greater than ...

... Mn/Ca variability also shows a relationship ... Cement II ... calcite concentration increases from cement ... Mn precipitation of Mn/Ca ratio ...

Figure 15: Minor element ratios of Fe/Ca and Mn/Ca for the calcite cement phases. Note that the majority of cements are depleted in both elements, except for Cement IV and V which are enriched in Mn and Fe respectively.

ratios occurring in the lower part of the section and the lowest ratios restricted to the upper part (Figure 13).

Cement IV lacks the stratigraphic variability observed in Cements I, II and III. Mg/Ca averages 6.0, ranging from 2.15 to 16.4; Sr/Ca averages 0.347, ranging from 0.162 to 0.560 (Figure 14); and Fe/Ca averages 2.43, ranging from 0 to 7.71. The Mn/Ca is greater than Cements I, II, and III with an average value of 0.704 and a maximum of 1.63 (Figure 15), which is consistent with the brightly luminescent character of this cement (Machel, 1985).

The Mg/Ca value of Cement V is 4.83, the lowest average of all cements, and less variable, ranging from 3.00 to 8.90. The average Sr/Ca of 0.390 for Cement V is still similar to Cement IV but is more variable with a range from 0.185 to 1.01 (Figure 14). This cement is Fe-rich with an average Fe/Ca value of 4.09, and a range from 1.90 to 16.3. The average Mn/Ca value is 0.278 which is less than Cement IV but greater than Cements I, II, and III (Figure 15).

Overall, a decreasing trend in the Mg/Ca ratios can be observed between Cement I to Cement V, while Fe concentrations increase from Cement I to Cement V. Mn concentrations increase from Cements I through IV, but decrease in Cement V. This is the opposite of Sr/Ca values that remain relatively constant among Cements I through IV, but slightly increase in Cement V.

RECONSTRUCTION OF THE DIAGENETIC HISTORY

Through analysis of the petrographic characteristics of the calcite cements, their stratigraphic location, and their geochemical signatures, it is possible to reconstruct the deposition, exposure, and alteration histories of the mound and associated deposits. A paragenetic sequence (Figure 16) was constructed based on the aforementioned characteristics and provides a record of the relative timing of the alteration events.

Diagenetic Episodes

Multiple episodes of diagenesis have been identified for the sediments comprising Yucca Mound, Leopard Knob, and the associated flanking beds and have been linked to the depositional history and stratigraphic relationships of the bioherms. Through detailed petrographic analysis coupled with stable isotopic and trace element analyses, four distinct stages of diagenesis were identified: Marine, Meteoric I, Meteoric II, and Burial.

Marine Diagenesis

This stage of diagenesis is inferred from the occurrence and petrographic characteristics of early Cement I, which is restricted to areas where primary porosity is present. This stage is evident as recrystallized marine calcite cement (Lohmann and Meyers, 1977) which precipitated in primary pores usually within skeletal debris, such as brachiopods (Figure 10). This calcite cement is interpreted to have developed in the marine diagenetic environment (James and Choquette, 1990a), after and during the deposition of the bioherms. Cementation was not extensive enough to completely occlude the primary pores, thus porosity remained and allowed for infiltration of meteoric water during exposure of the units.
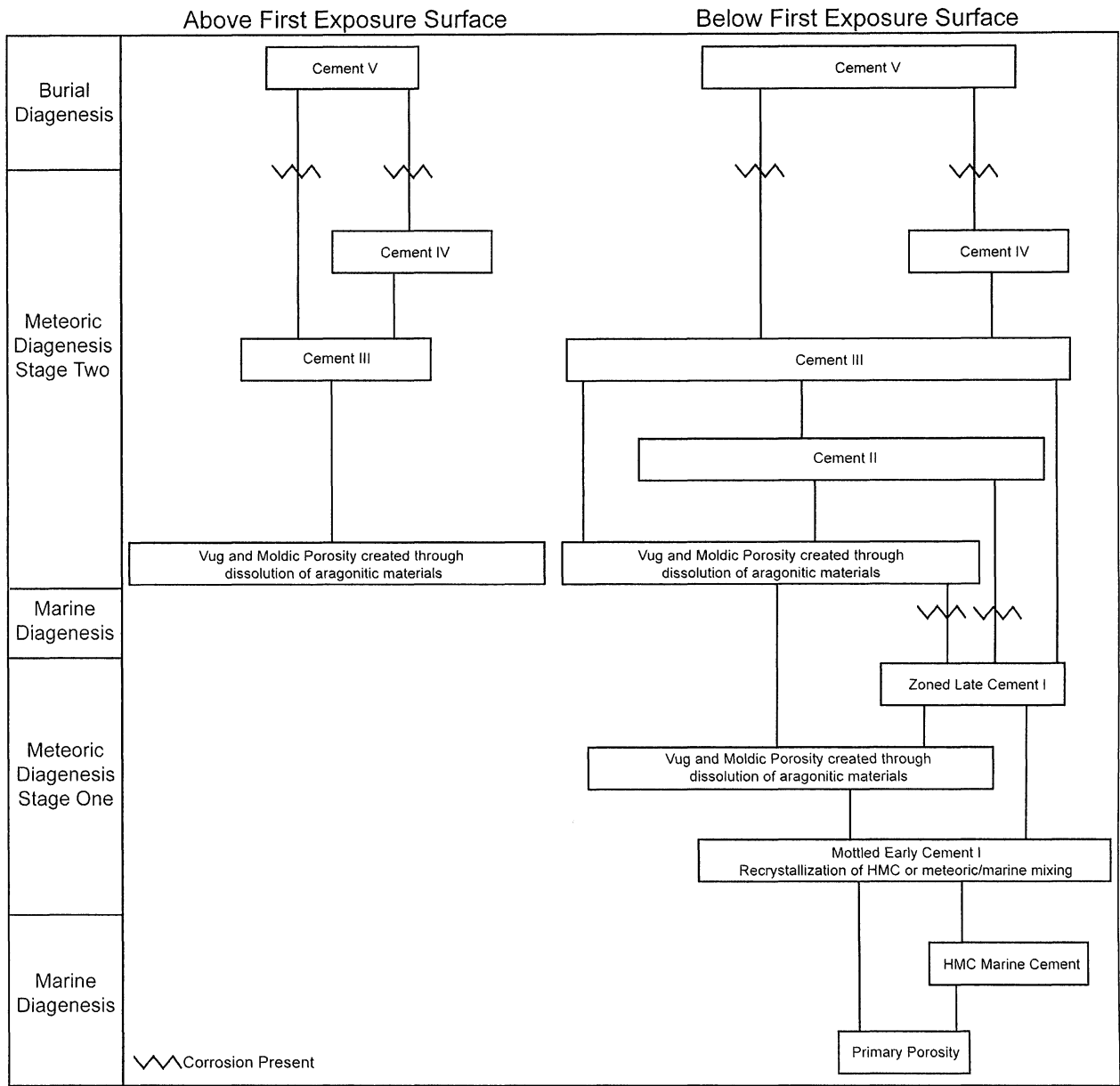
Figure 16: Paragenetic sequence summarizing the diagenetic patterns observed in the section. Diagenetic stages delineated on the left to separate the various materials removed and precipitated during each stage. Lines display successive cement phases and alteration events, and possible paths through which cement growth may have proceeded. Adapted from Benito et al. (2001).

38

Meteoric Diagenesis Stage One

The first period of meteoric diagenesis is associated with the stratigraphically lower subaerial exposure surface, identified based on the presence of a thin ferruginous zone within Yucca Mound (Figure 5). This exposure surface was not identified by Goldstein (1988a) because he identified exposure surfaces based exclusively on distinctive characteristics of paleosol development (i.e. rhizoliths, and alveolar textures), while in this study criteria of Wilson (1967) were used to identify ferruginous zones that were attributed to oxidation in a meteoric environment.

Cement I is the only precipitate derived from the meteoric water which altered the deposits during this stage of diagenesis (Figure 16). This cement is interpreted as the initial meteoric cement precipitated in primary and secondary porosity below the first exposure surface. The average $\delta^{18}O$ value for Cement I of -4.8‰ is interpreted as the value of the precipitates derived from the meteoric water that was dominant during this stage. Based on the lack of distinct indicators of vadose precipitation (James and Choquette, 1990b; Longman, 1980) this cement is interpreted as a meteoric phreatic precipitate. In many of the primary pores in which Cement I is precipitated, two distinct cathodoluminescent growth forms for this cement are evident. Early Cement I is highly mottled (Figure 11D), while late Cement I displays oscillatory cathodoluminescent zonation (Machel and Burton, 1991). The highly mottled nature of early Cement I can be interpreted in two ways. The first is that these cements represent recrystallized marine calcite cement (Land, 1970; Lohmann and Meyers, 1977). The cement displays isotopic values that trend toward the original Pennsylvanian marine calcite value (Figure 17) (Lohmann and Walker, 1987; Veizer, 1999; Mii, 1999), and has Mg/Ca ratios up to

two times as great as late Cement I, which lacks evidence of mottling (Figure 17). The isotopic and elemental data are equivocal, however, because not only can meteoric precipitates retain the marine signature from altered marine cements (Lohmann and Meyers, 1977), but the trends observed in the data are also common to cement precipitated in meteoric/marine mixing zones (Frank and Lohmann, 1995; Frank et al., 1995; Meyers and Lohmann, 1978).

The mixed-water interpretation for the development of early Cement I is based on the mixing of meteoric and marine water in the lower deposits of the section. Based on the Ghyben-Herzberg relationship (freshwater can penetrate to a depth up to 40 times as great as the fresh water table lies above sea-level (Goldstein, 1986; Buddemeier and Oberdorfer, 1986)), and the fact the cements lie very close to the exposure surface, this early cement may have formed prior to full exposure of the unit, while brackish water developed in the sediments close to the sediment/water interface due to processes of tidal-pumping and convection (Burnett et al., 2003, Figure 1). Regardless of the process of early alteration, the marine signature in early Cement I is small, and is dominated by the meteoric end member of -4.8‰ $\delta^{18}O_{VPDB}$ (Figure 12).

During this stage of diagenesis, vuggy and moldic porosity developed by removal of metastable carbonate material (i.e. aragonite), and was later rimmed by Cement I. The optical properties of cement precipitated in this secondary porosity are distinct when compared to that precipitated in primary porosity. Primary porosity is commonly isopachously coated with early Cement I. Early Cement I is then coated with late Cement I, which is the only cement observed rimming secondary vuggy and moldic
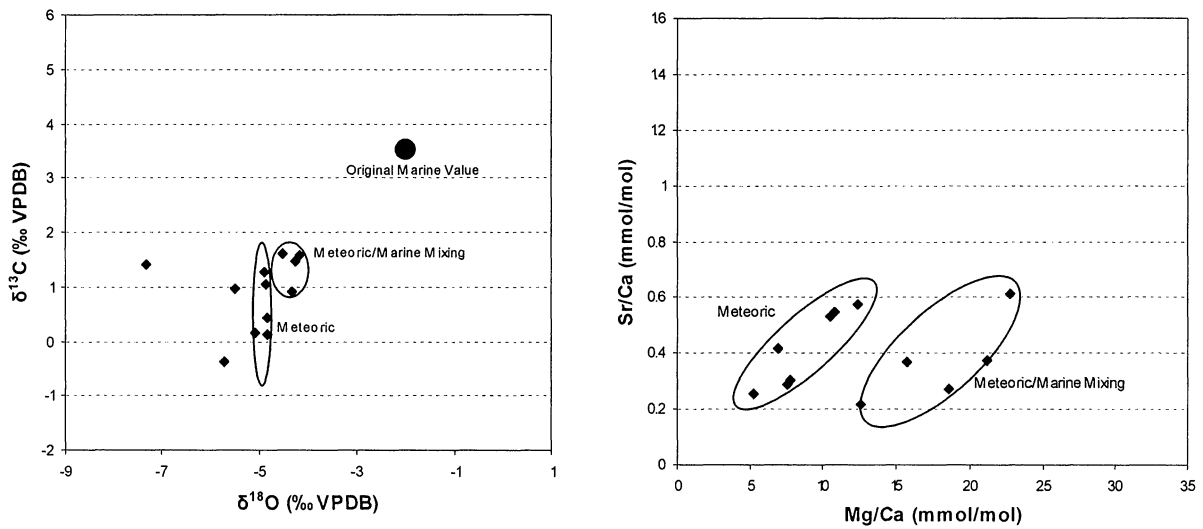
Figure 17: Isotopic and elemental (Sr and Mg) concentrations of Cement I, displaying fields interpreted as meteoric/marine mixing and meteoric. Early Cement I is mottled, and tends to have geochemical signatures that reside within the meteoric/marine mixing field. The mixing of meteoric and marine waters may be the cause of the mottled nature of the cements, along with the higher oxygen, carbon, and Mg values of the cement. Late Cement I tends to have a geochemical signature restricted to the meteoric field.

porosity formed during this stage of diagenesis, and has isotopic values close to the average $\delta^{18}O$ (-4.8‰), which is interpreted as the meteoric signature.

Meteoric Diagenesis Stage Two

The second stage of meteoric diagenesis is associated with the second subaerial exposure surface (Figure 5), which is the initial exposure surface for the unit recognized by Goldstein (1986; 1988a and b; 1991), and displays laminated crusts rich in rhizoliths (Figure 18). Three phases of cement are associated with the second episode of exposure. Due to the lack of vadose cement fabrics, these cements are interpreted to have precipitated in a phreatic environment.

Cement II and Cement III are the main precipitates derived from the meteoric waters of this meteoric diagenetic stage. When combined, the isotopic data from these two cement phases have an average of -5.6‰ $\delta^{18}O_{VPDB}$, and show a vertical trend in $\delta^{13}C$ at this average, thus displaying a meteoric calcite line for this stage of diagenesis (Figure 12). The $\delta^{13}C$ values range from -1.58 to 5.23‰, with Cement III comprising the majority of data below 1‰; whereas, Cement II comprises the majority of the data between 1 to 3‰. Cement II also has higher Mg/Ca and Sr/Ca ratios on average than Cement III (Figures 12 & 14). Cement II is also only present 10 meters or more below the second exposure surface, in the lower deposits of Yucca Mound and within Leopard Knob. Based on the stratigraphic distribution of Cement II, the increased concentrations of minor elements, and more positive $\delta^{13}C$ values, this cement phase is interpreted as a precipitate from meteoric water during the initial alteration of this stage of diagenesis. The cement was precipitated from meteoric water that passed through the mound,
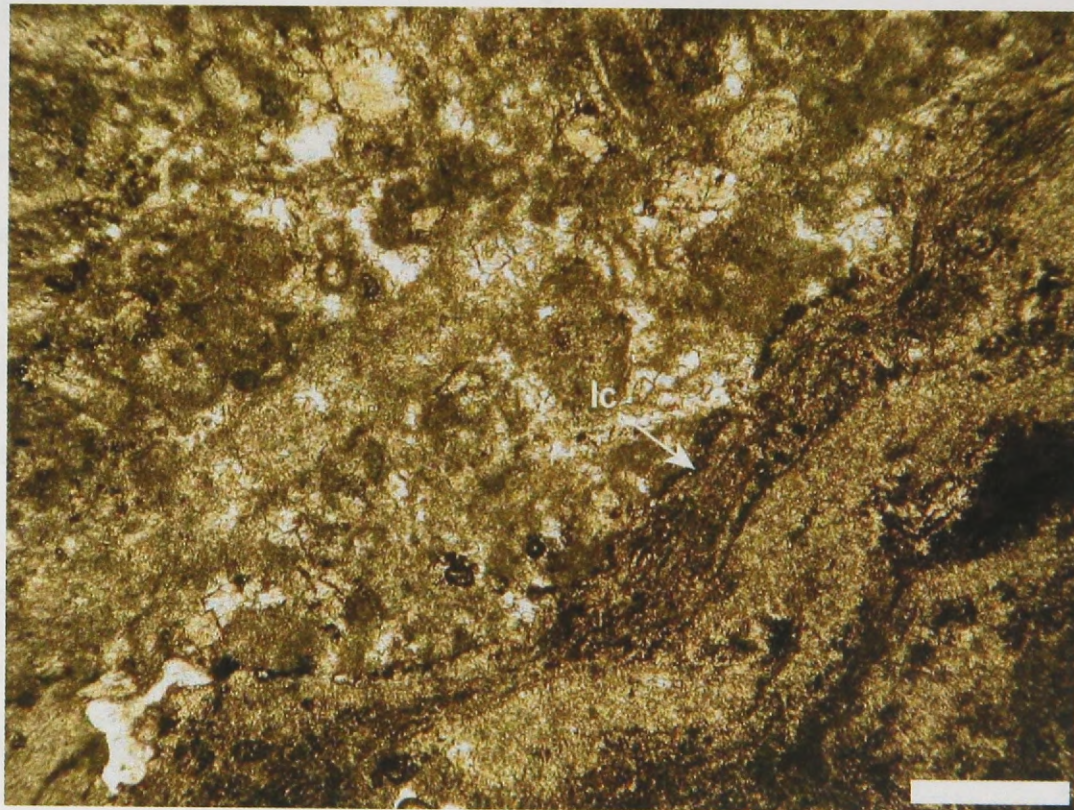
Figure 18: Thin section photomicrograph of material taken from subaerial exposure surface two, which is associated with meteoric diagenesis stage two. Note development of laminated crusts (lc) rich in rhizoliths (Goldstein, 1988a). Scale bar is 500 μm in length.

43

dissolving much of the metastable carbonate elements, and displaying carbon isotopic values close to the primary marine calcite.

Lohmann (1988) proposed a model that suggests during early meteoric diagenesis of carbonate material, a meteoric cement phase will be precipitated, distally from the exposure surface within the meteoric lens, that displays isotopic and elemental geochemistry dominated by that of the original marine precipitates. This occurs because as meteoric water passes through carbonate material, it reacts with metastable marine components, thus evolving to chemistry similar to that of the material being dissolved. During the early stages of diagenesis, metastable components are reactive carbonate phases, and thus meteoric water has an abundance of carbonate with which to react, and thus their chemistry can become dominated by the dissolving rock compositions. Precipitates from this rock-dominated meteoric water will display both isotopic and elemental compositions that reflect the chemistry of the carbonate that has reacted with this water. Based on this model of diagenesis, Cement II is a precipitate from the rock-dominated phase of meteoric water that altered the sequence early during the second stage of diagenesis. Because this phase precipitated further within the meteoric system from the second exposure surface, as compared to Cement III, it is predicted that it should display higher $\delta^{13}C$, Mg/Ca, and Sr/Ca values.

However, as diagenesis continues, the metastable components are increasingly removed, and reactive meteoric water has less material to dissolve, and the water retains its original low rock/water geochemistry. Thus, precipitates from successive parcels of meteoric water should display progressively more water-dominated geochemistry versus the rock-dominated geochemistry characteristic of precipitates

44

from earlier meteoric diagenesis (Lohmann, 1988, Figure 2.11). Cement III likely represents the water-dominated precipitate from this stage of meteoric diagenesis.

Importantly, this phase of cement is present throughout the whole unit and is the dominant meteoric cement above 10 meters depth in the section. Open system diagenesis appears to be the dominant process during the later part of this stage of meteoric diagenesis when Cement III developed (Veizer, 1983). First, the cement displays a meteoric oxygen signature, characterized by a large range in $\delta^{13}C$ values, with the lowest values at the second exposure surface and increasing at depth (Figures 12 & 13). In an open system, where a meteoric lens is well established, the soil gas CO_2 signature will be recorded in precipitates of the upper few meters of the section. However, this negative $\delta^{13}C$ signature attenuates with distance from the exposure surface as meteoric water equilibrates with the original rock value in response to increased rock-water interaction (Frank and Lohmann, 1995; Allan and Matthews, 1982). Second, concentrations of Mg and Sr in Cement III are the lowest (on average) of all interpreted meteoric phases (Figures 13 & 14), with these elements increasing in concentration with distance from subaerial exposure surface two (Figures 5 & 13). Elemental concentrations are commonly low in systems reflecting low rock-water interaction, as such these systems characteristically precipitate cements low in incompatible elements, (i.e., Mg and Sr), and typically are highly oxidizing (Veizer, 1983). Lastly, studies have shown that non-luminescent cements that contain low concentrations of both Fe and Mn, which are then followed by a brightly luminescent phase, are indicative of a highly oxidizing environment (Barnaby and Rimstidt, 1989; Emery and Dickson, 1989; Machel, 1985; Machel, 2000) that with time becomes

progressively more reduced. Cement III, which is low in Fe and Mn, is overlain by brightly luminescent Cement IV. As the meteoric system evolved and the majority of the metastable carbonate components had been dissolved, meteoric water with a water-dominated geochemistry infiltrated to greater depths (Meyers and Lohmann, 1985). From this water, Cement III began to precipitate at depth (up to 30 meters) on Cement II, which reflects the shift in the degree of rock-water interaction that reflects the evolution of the diagenetic system from a rock-dominated to a water-dominated geochemical system.

Moldic and vuggy porosity was created (Figure 16) during this episode of subaerial exposure, and much of this porosity, as well as porosity remaining from the first stage of meteoric diagenesis, was occluded by Cement II and Cement III. Porosity that remained was occluded by a combination of Cements IV and V. The precipitation of cement that was highly zoned, as observed under CL (Figure 11E), must reflect variation in the degree of system closure (flow rate versus reaction rate; M. Benito, personal communication, 2005), reduced rates of precipitation, or an increase in the reductive potential of the water (Machel and Burton, 1991; Barnaby and Rimstidt, 1989; Veizer, 1983). As the reductive potential of the meteoric water increased, oscillatory zonation gave way to Cement IV precipitation, which is higher in both Mn and Fe than the meteoric cement phases. Reduction of precipitating waters is not the only process, however, which can increase Mn and Fe concentrations in cement. An increase in the temperature of precipitation or a decrease in the rate of precipitation, are both possible alternatives that characterize the conditions of Cement IV precipitation (Barnaby and Rimstidt, 1989; Dromgoole and Walter, 1990). Mn and Fe concentrations are equivocal,

and could reflect a combination of all three processes. However, the decrease in $\delta^{18}O$ associated with Cement IV suggests that an increase in temperature is the most likely cause of this increase in Fe and Mn (Choquette and James, 1990).

Cement IV displays an average $\delta^{18}O_{VPDB}$ value of -6.3‰, which is almost a 1‰ decrease from Cements II and III, and is ascribed to minor burial and mixture of meteoric waters with connate waters in a closed system (Veizer, 1983). These data provide an argument for an increase in temperature, but do not rule out either other possibility as a cause for the increase in Mn and Fe concentration. Most likely, a combination of a reducing environment and an increase in temperature (Machel, 2000; Veizer, 1983) led to the conditions under which Cement IV precipitated.

Burial Diagenesis

The final stage of alteration evident in the sequence of calcite cements observed in the deposits is burial diagenesis. Based on petrographic descriptions of burial cement by Choquette and James (1990), Grover and Read (1983), Moore and Druckman (1981), and Dorobek (1987), it is evident that Cement V was precipitated late and under conditions of increasing burial. Not only is Cement V coarsely crystalline calcite, but it displays a highly mottled, dull-orange luminescence, that is associated with the presence of fluid inclusions (Goldstein, 1986). The cement is commonly massive, lacking distinct CL zonation, but can exhibit subtle zoning (Figure 11C, D, E, and F). Cement V is also observed occluding fractures which heal broken micrite envelopes of replaced phylloid-algae or earlier precipitated equant cements (Figure 19), features that commonly develop during burial and compaction (Choquette and James, 1990). Furthermore, Cement V displays the most negative $\delta^{18}O$ values of all cement

phases, with an average of -7.3‰, ranging down to -8.6‰ (Figure 12). Cements

precipitated from burial fluids at elevated temperatures commonly display very negative

$\delta^{18}O$ values (e.g. Benito et al, 2001; Choquette and James, 1990; Moore and

Druckman, 1980; Dorobek, 1987). Elemental analysis of Cement V displays elevated

Fe concentrations, up to 10 times that of the previous cement phases (Figure 15). High

Fe concentrations have been observed in interpreted burial cements by Benito et al.

(2001), Dorobek (1987), and Niemann and Read (1988). High Fe contents have been

attributed to either an increase in redox potential of burial waters, which activate

available, reducible Fe from sedimentary oxides (Barnaby and Rimstidt, 1989; Emery

and Dickson, 1989), or from an increase in incorporation of Fe^{2+} into the calcite crystal

lattice due to an increase in temperature (Dromgoole and Walter, 1990). Most likely, a

combination of the two processes led to the enrichment of Fe observed in Cement V.

Conditions of burial must have shifted the saturation of burial waters as earlier

precipitated low-Mg calcite cements exhibit evidence of dissolution of previous cement

phases manifested as corrosive boundaries between Cement IV and V, with the

complete removal of Cement IV locally (Figure 11 B, C, & D). Lastly, during this final

stage of diagenesis, all remaining porosity was occluded with the precipitation of
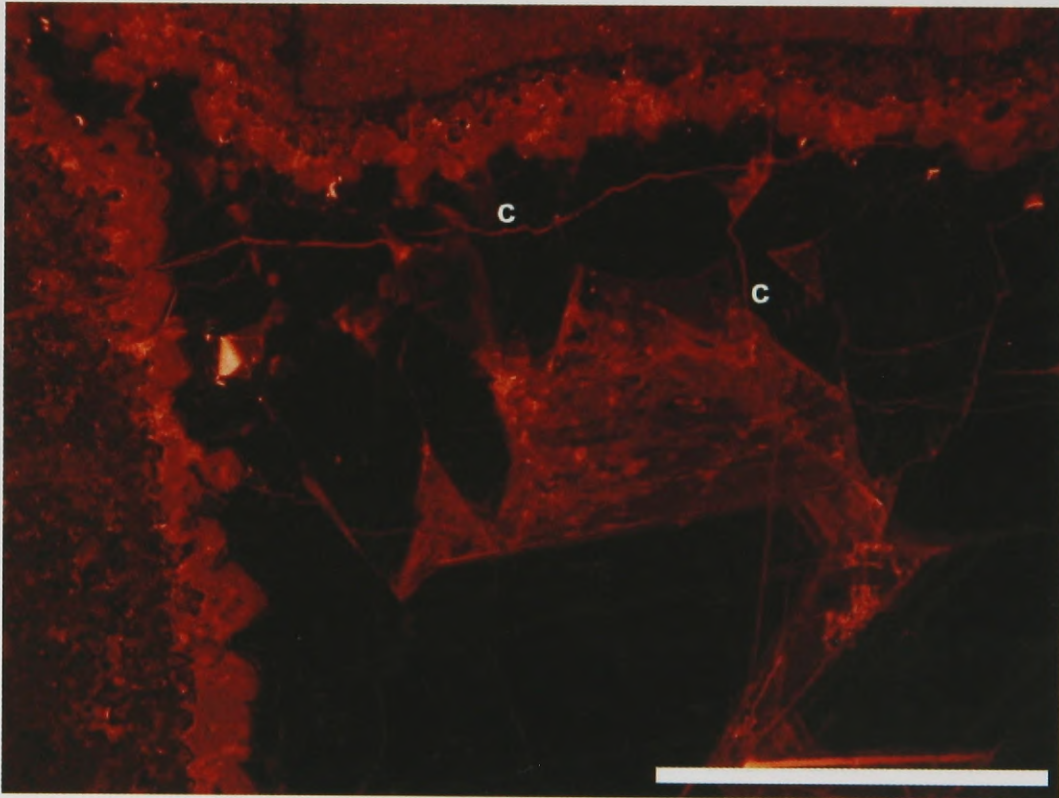
Cement V.

Figure 19: Cathodoluminescent photomicrograph displaying Cement V occluding porosity created by cracks (c) in the sample. Note how all previous phases are crosscut by the cement within the cracks except Cement V, at which all cracks appear to terminate. Scale bar is 500 µm in length.

Numerical Modeling of Elemental and Isotopic Geochemistry

By analyzing the minor element content (i.e. Mg, Sr, Fe, and Mn) of multiphase meteoric cements, previous workers (e.g. Meyers and Lohmann, 1978; Dorobek, 1987; Meyers, 1989; Saller and Moore, 1991) have been able to infer the diagenetic settings in which carbonate sequences have been altered. Such analysis has led to minor element models that, when paired with petrographic observations, provide insight into how these settings control the spatial and temporal patterns of elemental chemistry (Lohmann, 1988; Meyers, 1989; Veizer, 1983; Cicero and Lohmann, 2001; James and Choquette, 1990a and b).

A model was constructed to simulate the paired response of the elemental and isotopic tracers in a meteoric system and then compare to patterns observed in the diagenetic record of Yucca Mound and associated deposits. The model, based on prior work of Mucci and Morse (1983), Veizer (1983), and Cicero and Lohmann (2001), calculates changes in cement composition with increasing rock-water interaction to determine the rock/water (R/W) ratios at which individual tracers progress from open to closed system behaviors. Comparison of predicted cement compositions among multiple model runs, which varied the initial starting compositions and elemental distribution coefficients, with the observed values and variation present within the cements, allows estimation of the original composition of the sediments comprising the deposits.

Carbon isotope values, elemental concentrations, and the elemental distribution coefficients were varied to represent differences in the initial sediment mineralogy, and in the diagenetic environments. Carbon values for the altering water (meteoric water)

were varied between -25 to -4‰ $\delta^{13}C_{VPDB}$, to accommodate variation that could result from differences in soil development and duration of exposure. Ranges in the concentrations of Mg and Sr were used in the model to simulate the spectrum of initial carbonate mineralogies (i.e. low-Mg calcite, high-Mg calcite, and aragonite) possible for the unaltered mound material. Mg was varied between 7,000 to 30,000 ppm, or 4 to 12 mole%, while Sr was varied between 1,300 to 5,000 ppm, or 0.1 to 0.5 mole%. Finally, based on analytical work by Carpenter et al. (1991) and Carpenter and Lohmann (1992), a range of distribution coefficients for both Mg (0.012-0.126) and Sr (0.026-0.14) was used to determine which reproduced the values found during elemental analysis of cement phases.

Maximum and minimum $\delta^{13}C$ values for each stage of meteoric diagenesis were used to constrain the boundaries over which the R/W ratio varied. These boundaries were then defined as upper and lower limits for the R/W ratio in model runs. By tuning the ratio based on run results, the R/W ratios over which each stage of meteoric diagenesis precipitated were determined and are low (maximum of 0.0057), requiring a system dominated by meteoric water in which little of the original rock composition is retained in the chemistry of precipitated cements (Figure 20).

Furthermore, concordance of model results with observed values was best with an initial composition of mound carbonate having a bulk Mg concentration of 14,700 ppm (6 mole%) and Sr concentration of 2,100 ppm (0.235 mole%), using distribution coefficients of 0.035 and 0.026 respectively. These values suggest original marine components composed of high-Mg calcite and aragonite, with some low-Mg calcite. This finding is contrary to previous work done on Yucca Mound and the Holder
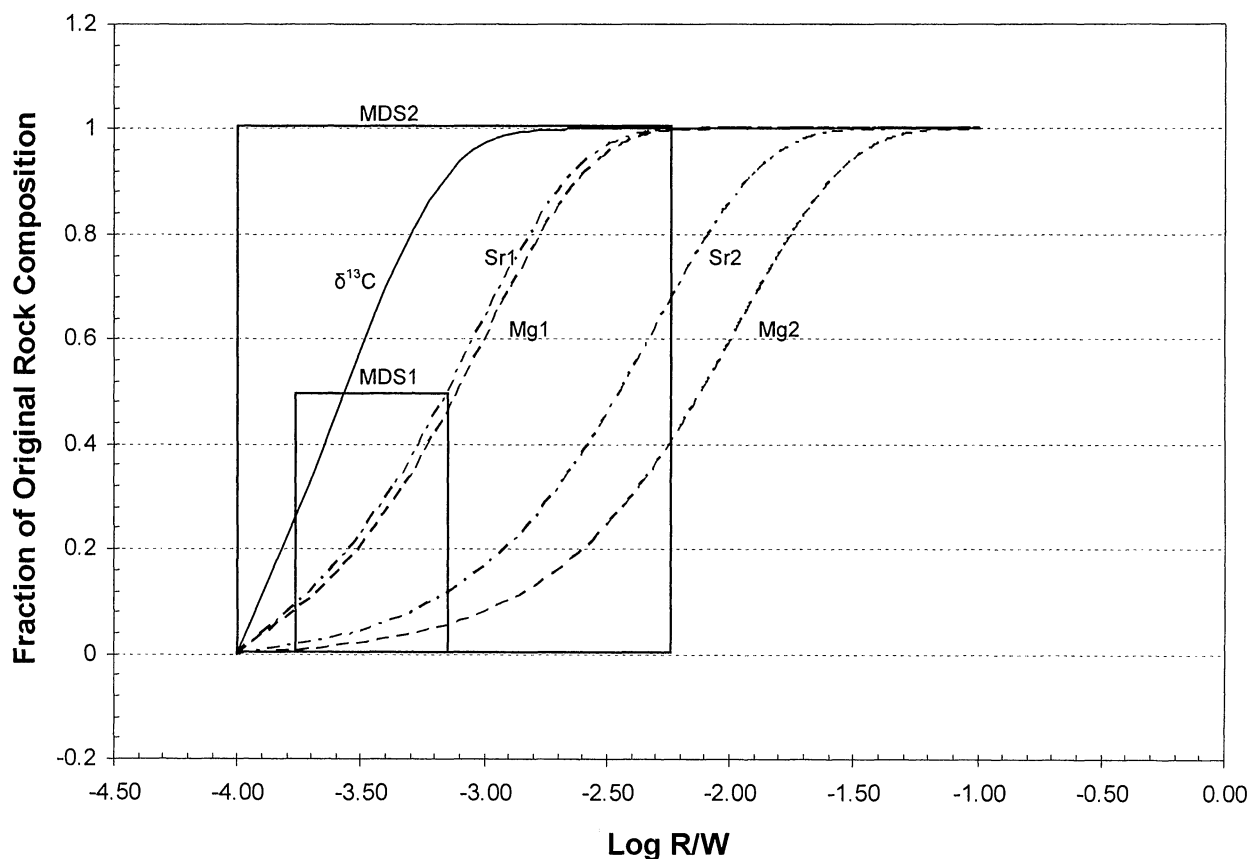
Figure 20: Plot displaying log of the rock/water ratio versus the fraction of original rock composition for model runs using the ideal calculated compositions of 6 mole% Mg and 0.235 mole% Sr. MDS1 and MDS2 refer to the range of values over which meteoric diagenesis stage 1 and 2 precipitated. It can be noted that both boxes are dominant over the ranges for which the elements and $\delta^{13}C$ are still considered open, which is prior to when the systems reach an original rock composition of 1 or 100%. The multiple lines for both Sr and Mg refer to model runs during which the distribution coefficients for the elements were varied between the minimum and the maximum used in this analysis (Sr1,D_{Sr}=0.14; Sr2,D_{Sr}=0.026; Mg1,D_{Mg}=0.126; Mg2,D_{Mg}=0.012). A full range of solutions is possible between each elemental line pair depending on the distribution coefficient used. Adapted from Cicero and Lohmann (2001).

Formation, in which it was assumed the material was mostly aragonitic due to the presence of original marine aragonite cements (Dickson et al., 1991), and the observation that phylloid-algae were also composed of aragonite (Kirkland et al., 1993). This study concludes that the micrite in the mound was a mixture of aragonite, with high and low-Mg calcite. Based on work by Gischler and Zingeler (2002) and Whittle et al. (1993), it has been shown that modern lime mud off of Belize and the Bahamas can contain low Sr concentrations, down to 2,174 ppm in Belize and down to 5,510 ppm in the Bahamas. Furthermore, carbonate mud off of Belize can contain up to 25.3% low-Mg calcite, 43.1% aragonite and 31.6% high-Mg calcite, with these percentages corresponding to bulk carbonate elemental contents of 15,523 ppm Mg and 2,174 ppm Sr. These values are similar to the initial elemental contents for bulk mound carbonate estimated from the numerical model. Since the late Pennsylvanian has been used as an ancient analogue to the modern, representing a time of aragonite seas (Sandberg, 1983; Dickson, 2004), widespread glaciation (Heckel, 1983), and Mg/Ca ratios similar to today's seawater, similarities in bulk rock composition are reasonable. The abundance of low-Mg calcite comprising the micrite may have been derived from benthic and encrusting foraminifers that are common throughout the unit. These foraminifers have been interpreted as low-Mg calcite due to the lack of obvious alteration with preservation of skeletal microfabrics.

DISCUSSION

Depositional History of the Holder Formation Inferred from Patterns of Diagenesis

Based on the sequence of diagenetic events present in the stratigraphic succession at Yucca mound, it is possible to infer aspects of the history of deposition and exposure in response to sea level fluctuations. Constraining the time over which these deposits were emplaced and altered is difficult. Previous work of Toomey (1981) and Soreghan and Giles (1999), suggest that bioherm growth and development was rapid, occurring over a short interval of time during the early Virgilian. Deposition of Yucca Mound was initiated with growth of the lower mound prior to the first episode of subaerial exposure (Figure 21). During this time, sea-level was relatively high and flooded most of the ancient Sacramento Shelf (Figure 5). As mound growth proceeded, marine waters inundated the bioherm and marine cementation dominated in primary porosity. During the rapid growth, relative sea-level must have lowered as evidenced by conditions that are reflected in the sediment formed in interbiohermal areas (Toomey et al., 1977). Within these interbiohermal settings, the leopard rock facies was formed that is characterized by fauna that suggest a restricted marine setting with elevated salinity conditions. It has been proposed that Leopard Knob formed in such a restricted setting on the western flank of Yucca Mound, along with thin, flanking beds which overlie this small biohermal mound. Alteration during the first period of exposure is apparent in the precipitation of early Cement I from meteoric waters which either altered existing marine cements or formed as an initial stage of meteoric/marine mixed water calcite within Leopard Knob and the lower deposits of Yucca Mound. The extent of marine water mixing during this exposure event must have been relatively minor given the small
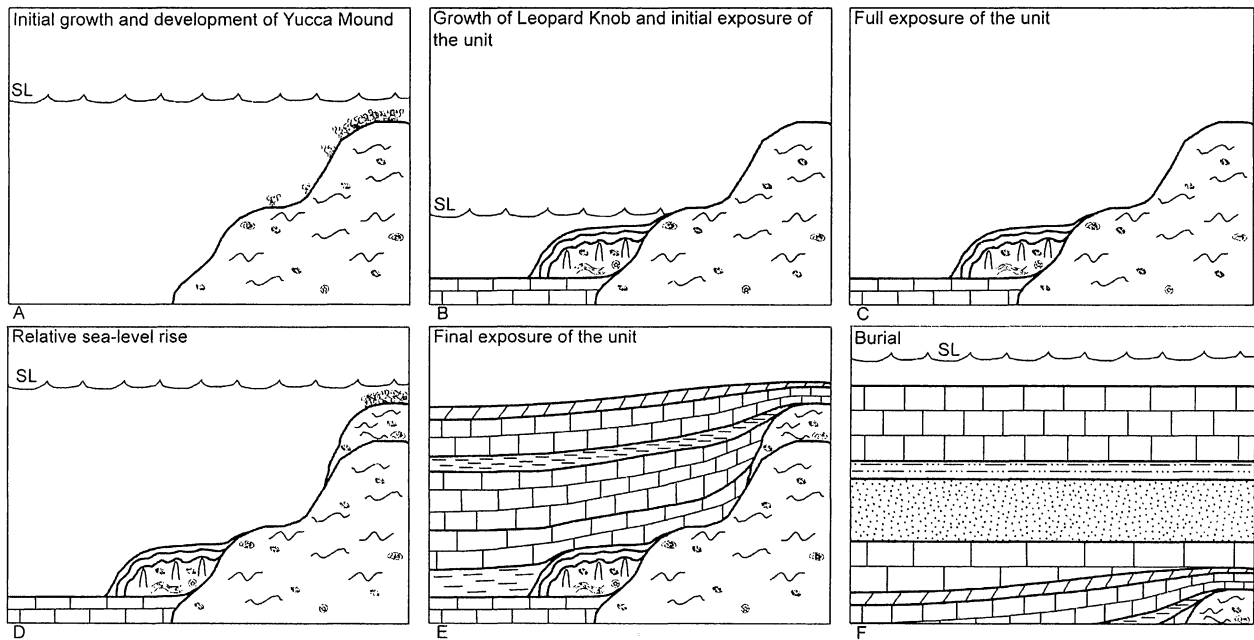
Figure 21: Diagram summarizing the order of depositional events which formed Yucca Mound and related deposits. A. Deposition of Yucca Mound. B. Relative sea-level fall, with growth of Leopard Knob, the leopard rock facies (Toomey et al., 1977), and exposure of the upper portions of the existing Yucca Mound complex. C. Full exposure of the unit during which late Cement I precipitated. D. Rise in relative sea-level and deposition of the remainder of Yucca Mound, and the flanking deposits overlying the mound. E. Second subaerial exposure, during which Cement II and Cement III precipitated. F. Rise in relative sea-level, and burial of the unit. Adapted from Benito et al. (2001).

difference between the $\delta^{18}O$ values of the meteoric calcites of late Cement I relative to the mixed water cements represented by early Cement I (Figure 17). Complete exposure of Leopard Knob and the lower part of Yucca Mound is represented by late Cement I which has an average $\delta^{18}O_{VPDB}$ = -4.8‰. The absence of a definitive soil zone associated with the first exposure surface, however, suggests the duration of this event was relatively short.

Exposure of the mound and flanking bed sequence is followed by a relative sea-level rise as indicated by the resumption of growth of the mound and deposition on the nearby shelf. As sea-level rose, growth of Yucca Mound initially occurred in shallow water based on the abundance of phylloid-algae. Water depth, however, must have increased during deposition of the upper part of Yucca Mound as flanking beds were subsequently deposited on top and across the flanks of the mound (Soreghan and Giles, 1999).

The second episode of subaerial exposure occurred after deposition of about 10 meters of flanking beds on top of the mound. The drop of sea-level associated with this exposure event must have been rapid as the leopard rock facies is absent in the interbiohermal areas. During this stage of exposure, an extensive meteoric lens must have been developed as Cements II and III were precipitated throughout the stratigraphic section beneath the second exposure surface which is marked by a horizon with extensive development of soil features. Based on the variation in $\delta^{13}C$ of Cements II and III along the meteoric calcite line at = -5.6‰ $\delta^{18}O$ (Goldstein, 1986, 1991; Fernberg, 1987), diagenesis must have occurred under conditions of a relatively open, water dominated system. In addition, this second event of meteoric alteration is

manifest in the formation of extensive secondary, moldic and vuggy porosity which developed through the dissolution of aragonitic micrite and skeletal allochems. Toward the end of exposure, permeability of the unit dropped, and closed system diagenesis began to dominate, with an increase in the reductive potential of reactive waters a likely process (Veizer, 1983).

After precipitation of Cement III, there is a gradual transition to Cement IV precipitation evidenced by oscillatory zonation between the phases. Cement IV has high concentrations of both Mn and Fe, relative to the other cement phases, and an average $\delta^{18}O$ = -6.3‰, which is more negative than the previous phases. Based on the geochemical data and the gradual transition between the cement phases, Cement IV precipitated during shallow burial under conditions of increasing temperature. A burial setting for Cement IV is also supported by increases in Fe and Mn contents which could reflect a shift toward reducing conditions as flow within the meteoric system waned.

Burial continued as subsidence and deposition of overlying units occurred, and is recorded by the emplacement of Cement V which constitutes the final period of the bioherms' diagenetic history. Constraining the temperature conditions and fluid sources during burial is difficult. Estimates of the maximum burial temperatures for the Holder Formation vary between studies, from ~50 to 60°C (Algeo et al., 1992) to greater than 97°C (Goldstein, 1986). The burial depth and temperature of precipitation of Cement V can be estimated based on an assumption of the $\delta^{18}O$ composition of the diagenetic water. The $\delta^{18}O$ value of the calcite formed during the final stage of meteoric exposure is -5.6 ‰. If it is assumed that this meteoric water remained as the interstitial fluids responsible for burial diagenesis, the difference in $\Delta^{18}O$ composition between the

meteoric and burial calcites can be used to calculate the increase in fluid temperature. Given that the meteoric calcite was formed at or near the surface in an equatorial region, average groundwater temperatures likely ranged from ~20 to 25°C (Golonka, 2002). Using the fractionation equation of O'Neil et al. (1969) and the range of $\delta^{18}O_{VPDB}$ of Cement V from -7.3‰ to -8.6‰, the temperatures of precipitation would range from 35 to 40°C. Furthermore, using an average geothermal gradient of 30°C/km (Allen and Allen, 1990) a minimum burial depth of 500 m is required to reach those temperatures. These estimates of burial depth and temperature match closely with the burial history curve for the Orogrande Basin reconstructed by Algeo et al. (1992). This reconstruction suggests a period of rapid burial of the Holder Formation by up to 1 km of Permian-aged sediments, which is similar to conclusions reached by Pray (1961), and suggests that Cement V was likely emplaced during the early Permian.

Goldstein (1986) estimates up to 3 km of burial for the Holder Formation based on fluid inclusion analyses of burial cements, with most of that burial occurring post-Paleozoic. This estimate differs from this study because Goldstein identified the cement occluding Yucca Mound as entirely meteoric, while this study has identified one distinct burial phase among these cements. Post-Paleozoic burial certainly occurred, and may have been responsible for the conditions under which other burial cements developed; however, these cements are not present in Yucca Mound or its associated deposits.

CONCLUSIONS

The depositional and diagenetic history of the Yucca Mound complex, including flanking beds and associated bioherms, has been determined based on a detailed analysis of the petrographic and geochemical characteristics of calcite cements, precipitated from waters which altered the unit during its development.

- Five phases of cement were identified based on their cathodoluminescent and geochemical properties. Cement I can be mottled or highly zoned and is the initial cement rimming primary and secondary porosity. Cement I is only present below the first subaerial exposure surface in the unit. Cement II is dully luminescent and develops epitaxially to Cement I. Cement III is non-luminescent and, along with Cement II, precipitated from waters associated with the second subaerial exposure surface. Cement IV is brightly luminescent and is commonly corroded prior to precipitation of the mottled, dully luminescent Cement V.

- Based on comparisons between stratigraphic location, petrography, and geochemistry of the cement phases four stages of diagenesis have been identified. Marine diagenesis occurred while the mound was still developing below sea-level. During this time high-Mg calcite cement was precipitated within primary porosity. This cement is later recrystallized to the highly mottled early Cement I during meteoric diagenesis.

- Late Cement I is the meteoric cement precipitated during the first stage of meteoric diagenesis, which developed due to the first period of subaerial exposure. The average $\delta^{18}O_{VPDB}$ of -4.8‰ is the value of meteoric calcite precipitated during this stage of diagenesis.

- The second stage of meteoric diagenesis was recorded in Cement II and Cement III, which are interpreted as precipitates from the meteoric water associated with the second subaerial exposure surface. The average $\delta^{18}O_{VPDB}$ of -5.6‰ for the combined cement phases has been interpreted as the meteoric calcite line for the second stage of meteoric diagenesis (Lohmann, 1988), and is similar to previous conclusions reached in other studies of Yucca Mound (Fernberg, 1987; Goldstein, 1986, 1988a&b, 1991). Cement IV precipitated from the interstitial waters that remained in the sediments after permeability was decreased due to Cement II and Cement III precipitation. Based on a more negative $\delta^{18}O$ (-6.3‰) and increased Fe and Mn concentrations, Cement IV precipitated from waters with an increased reductive potential and increased temperatures, due to minor burial.

- Cement V precipitated during the final stage of diagenesis dominated by burial of the deposits. During this stage, undersaturated burial waters altered the sediments removing much of the previous meteoric cement, and precipitating Cement V in a reducing environment under increased temperatures.

- Minor element (Mg, Sr, Fe, and Mn) concentrations within the cements associated with each stage of diagenesis suggest various processes took place during these stages, such as open versus closed system diagenesis and oxidizing versus reducing conditions, which further reinforces the interpretations made based on petrography and stable isotope geochemistry.

- Modeling of the system based on an ideal diagenetic proxy has led to identification of the rock/water ratio (maximum 0.0057) over which meteoric

diagenesis occurred, further reinforcing an open diagenetic system for the two stages of meteoric diagenesis. Modeling has also shown that much of the original carbonate within Yucca Mound may not have been entirely aragonitic, but also included high-Mg calcite and low-Mg calcite constituents (up to 32% and 25% respectively).

- A depositional model for the unit was constructed. Initially, primary porosity was partially filled by high-Mg marine cements. During mound growth, sea-level dropped and in interbiohermal areas a leopard rock facies formed. This facies developed in a restrictive environment and includes Leopard Knob and its respective flanking beds. Associated with this period of exposure, meteoric cements were precipitated, as represented by late Cement I, but marine waters infiltrated into the exposed sections of the mound, and early Cement I was also emplaced due to meteoric/marine mixing. With an increase in relative sea-level, Yucca Mound continued growth, with several flanking beds developing on top of the mound. A second exposure surface developed, after sea-level fall, that displays soil formation. Cement II and Cement III are the meteoric cements precipitated during the second period of exposure. Marine water then inundated the deposits. Meteoric water associated with exposure remained in the pores, and Cement IV precipitated. During burial and deposition of overlying early Permian units, burial waters infiltrated the unit dissolving some cement, evident by corrosion, and Cement V precipitated. Conditions under which burial cementation occurred were shallow, at 500 m, and warm, 35-40°C.

REFERENCES

Algeo, T.J., Wilson, J.L., and Lohmann, K.C., 1991. Eustatic and Tectonic Controls on Cyclic Sediment Accumulation Patterns in Lower-Middle Pennsylvanian Strata of the Orogrande Basin, New Mexico. *In* J.M. Barker, B.S. Kues, G.S. Austin, S.G. Lucas, Geology of the Sierra Blanca, Sacramento and Capitan Ranges, New Mexico, NMGS 42nd Annual Field Conference, p.203-212.

Algeo, T.J., Wilkinson, B.H, and Lohmann, K.C, 1992. Meteoric-Burial Diagenesis of Middle Pennsylvanian Limestones in the Orogrande Basin, New Mexico: Water/Rock Interactions and Basin Geothermics. Journal of Sedimentary Petrology, v.62, n.4, p.652-670.

Allan, J.R. and Matthews, R.K., 1982. Isotope Signatures Associated with Early Meteoric Diagenesis. Sedimentology, v.29, p.797-817.

Allen, P.A. and Allen, J.R., 1990. Basin Analysis, Principles and Applications. Oxford, U.K., Blackwell, 451pp.

Barnaby, R.J. and Rimstidt, D.J., 1989. Redox conditions of calcite cementation interpreted from Mn and Fe contents of authigenic calcites. Geological Society of America Bulletin, v.101, p.795-804.

Benito, M.I., Lohmann, K.C., and Mas, R., 2001. Discrimination of Multiple Episodes of Meteoric Diagenesis in a Kimmeridgian Reefal Complex, North Iberian Range, Spain. Journal of Sedimentary Research, v.71, n.3, p.380-393.

Buddemeier, R.W. and Oberdorfer, J.A., 1986. Internal Hydrology and Geochemistry of Coral Reefs and Atoll Islands: Key to Diagenetic Variations. *In* J.H. Schroeder and B.H. Purser, Reef Diagenesis, p.91-111.

Burnett, W.C., Bokuniewicz, H., Huettel, M., Moore, W.S., and Taniguchi, M., 2003. Groundwater and pore water inputs to the coastal zone. Biogeochemistry, v.66, n.1-2, p.3-33.

Carpenter, S.J. and Lohmann, K.C., 1992. Sr/Mg ratios of modern marine calcite: Empirical indicators of ocean chemistry and precipitation rate. Geochimica et Cosmochimica Acta, v.56, p.1837-1849.

Carpenter, S.J., Lohmann, K.C., Holden, P., Walter, L.M., Huston, T.J., and Halliday, A.N., 1991. $\delta^{18}O$ values, $^{87}Sr/^{86}Sr$ and Sr/Mg ratios of Late Devonian abiotic marine calcite: Implications for the composition of ancient seawater. Geochimica et Cosmochimica Acta, v.55, p.1991-2010.

Choquette, P.W. and Pray, L.C., 1970. Geologic Nomenclature and Classification of Porosity in Sedimentary Carbonates. American Association of Petroleum Geologists Bulletin, v.54, n.2, p.207-250.

Choquette, P.W and James, N.P., 1990. Limestones – The Burial Diagenetic Environment. *In* I.A. McIlreath and D.W. Morrow eds., Diagenesis, p.75-112.

Cicero, A.D. and Lohmann, K.C, 2001. Sr/Mg variation during rock-water interaction: Implications for secular changes in the elemental chemistry of ancient seawater. Geochimica et Cosmochimica Acta, v.65, p741-761.

Craig, H., 1957. Isotopic Standards for Carbon and Oxygen and correction factors for mass spectrometric analyses of carbon dioxide. Geochimica et Cosmochimica Acta, v.12, p.133-149.

Dickinson, W.R. and Lawton, T.F., 2003. Sequential intercontinental suturing as the ultimate control for Pennsylvanian Ancestral Rocky Mountains deformation. Geology, v.31, n.7, p.609-612.

Dickson, J.A.D., 2001. Diagenesis and Crystal Caskets: Echinoderm Mg Calcite Transformation Dry Canyon, New Mexico, U.S.A. Journal of Sedimentary Research, v.71, n.5, p.764-777.

Dickson, J.A.D., 2004. Echinoderm Skeletal Preservation: Calcite-Aragonite Seas and the Mg/Ca Ratio of Phanerozoic Oceans. Journal of Sedimentary Research, v.74, n.3, p.355-365.

Dickson, J.A.D., Smalley, P.C., and Kirkland, B.L., 1991. Carbon and oxygen isotopes in Pennsylvanian biogenic and abiogenic aragonite (Otero County, New Mexico): A laser microprobe study. Geochimica et Cosmochimica Acta, v.55, p.2607-2613.

Dickson, J.A.D., Wood, R.A., and Kirkland, B.L., 1996. Exceptional Preservation of the Sponge *Fissispongia tortacloaca* from the Pennsylvanian Holder Formation, New Mexico. Palaios, v.11, p.559-570.

Dorobek, S.L., 1987. Petrography, Geochemistry, and Origin of Burial Diagenetic Facies, Siluro-Devonian Helderberg Group (Carbonate Rocks), Central Appalachians. American Association of Petroleum Geologists Bulletin, v.71, n.5, p.492-514.

Dromgoole, E. and Walter, L.M., 1990. Iron and manganese incorporation into calcite: Effects of growth kinetics, temperature, and solution chemistry. Chemical Geology, v.81, p.311-336.

Emery, D. and Dickson, J.A.D., 1989. A syndepositional meteoric phreatic lens in the Middle Jurassic Lincolnshire Limestone, England, U.K. Sedimentary Geology, v.65, p.273-284.

Fernberg, R.S., 1987. Diagenetic History of Cyclic Platform Sequences: Virgilian Holder Formation, Sacramento Mountains, New Mexico. Unpublished Masters Thesis, The University of Michigan, 39pp.

Frank, T.D. and Lohmann, K.C, 1995. Early Cementation During Marine-Meteoric Fluid Mixing: Mississippian Lake Valley Formation, New Mexico. Journal of Sedimentary Research, v.A65, n.2, p.263-273.

Frank, T.D., Lohmann, K.C, and Meyers, W.J., 1995. Chronostratigraphic significance of cathodoluminescence zoning in syntaxial cement: Mississippian Lake Valley Formation, New Mexico. Sedimentary Geology, v.105, p.29-50.

Gischler, E. and Zingeler, D., 2002. The origin of carbonate mud in isolated carbonate platforms of Belize, Central America. International Journal of Earth Sciences, v.91, p.1054-1070.

Goldstein, R.H., 1986. Integrative Carbonate Diagenesis Studies: Fluid Inclusions in Calcium Carbonate Cement; Paleosols and Cement Stratigraphy of Late Pennsylvanian Cyclic Strata, New Mexico. Ph.D. Dissertation, University of Wisconsin-Madison. 343 pp.

Goldstein, R.H., 1988a. Paleosols of Late Pennsylvanian cyclic strata, New Mexico. Sedimentology, v.35, p.777-803.

Goldstein, R.H., 1988b. Cement Stratigraphy of Pennsylvanian Holder Formation, Sacramento Mountains, New Mexico. American Association of Petroleum Geologists Bulletin, v.72, n.4, p.425-438.

Goldstein, R.H., 1991. Stable Isotope Signatures Associated with Palaeosols, Pennsylvanian Holder Formation, New Mexico. Sedimentology, v.38, p.67-77.

Golonka, J., 2002. Plate-Tectonic Maps of the Phanerozoic. In W. Kiessling, E.Flügel, J. Golonka, eds., Phanerozoic Reef Patterns, SEPM Special Publication #72, p.21-76.

Grover, G.Jr. and Read, J.F., 1983. Paleoaquifer and Deep Burial Related Cements Defined by Regional Cathodoluminescent Patterns, Middle Ordovician Carbonates, Virginia. The American Association of Petroleum Geologists Bulletin, v.67, n.8, p.1275-1303.

Heckel, P.H., 1983. Diagenetic model for carbonate rocks in mid-continent Pennsylvanian eustatic cyclothems. Journal of Sedimentary Petrology, v.53, p.733-760.

James, N.P. and Choquette, P.W., 1990a. Limestones – The Sea-Floor Diagenetic Environment. *In* I.A. McIlreath and D.W. Morrow eds., Diagenesis, p.13-34.

James, N.P. and Choquette, P.W., 1990b. Limestones - The Meteoric Diagenetic Environment. *In* I.A. McIlreath and D.W. Morrow eds., Diagenesis, p.35-74.

Kirkland, B.L., Moore, C.H. Jr., and Dickson, J.A.D., 1993. Well Preserved, Aragonitic Phylloid Algae (*Eugonophyllum*, Udotoeaceae) from the Pennsylvanian Holder Formation, Sacramento Mountains, New Mexico. Palaios, v.8, p.111-120.

Konishi, K. and Wray, J.L., 1961. *Eugonophyllum*, a new Pennsylvanian and Permian Algal Genus. Journal of Paleontology, v.35, n.4, p.659-666.

Land, L.S., 1970. Phreatic versus Vadose Meteoric Diagenesis of Limestones: Evidence from a Fossil Water Table. Sedimentology, v.14, p.175-185.

Lohmann, K.C., 1988. Geochemical Patterns of Meteoric Diagenetic Systems and their Application to Studies of Paleokarst. *In* N.P. James and P.W. Choquette, eds., Paleokarst: Berlin, Springer-Verlag, p.58-80.

Lohmann, K.C. and Meyers, J.M., 1977. Microdolomite Inclusions in Cloudy Prismatic Calcites: A proposed Criterion for Former High-Magnesium Calcites. Journal of Sedimentary Petrology, v.47, n.3, p.1078-1088.

Lohmann, K.C. and Walker J.C.G., 1989. The $\delta^{18}O$ Record of Phanerozoic Abiotic Marine Calcite Cements. Geophysical Research Letters, v.16, n.4, p.319-322.

Longman, M.W., 1980. Carbonate Diagenetic Textures from Nearsurface Diagenetic Environments. American Association of Petroleum Geologists Bulletin, v.64, n.4, p.461-487.

Machel, H.G., 1985. Cathodoluminescence in Calcite and Dolomite and its Chemical Interpretation. Geoscience Canada, vol.12, no.4, pp.139-147.

Machel, H.G., 2000. Chapter 11: Application of Cathodoluminescence to Carbonate Diagenesis. *In* M. Pagel, V. Barbin, P. Blanc, and D. Ohnenstetter, eds., Cathodoluminescence in Geosciences. Springer-Verlag, Berlin, p.271-302.

Machel, H.G. and Burton, E.A., 1991. Factors Governing Cathodoluminescence in Calcite and Dolomite, and Their Implications for Studies of Carbonate Diagenesis. *In* C.E. Barker and O.C. Kopp, eds. Luminescence Microscopy and Spectroscopy:

Qualitative and Quantitative Applications. SEPM Short Course 25, Dallas, Texas, p.37-57.

Meyers, W.J., 1989. Trace element and isotope geochemistry of zoned calcite cements, Lake Valley Formation (Mississippian, New Mexico): insights form water-rock interaction modeling. Sedimentary Geology, v.65, p.355-370.

Meyers, W.J. and Lohmann, K.C., 1978. Microdolomite-rich syntaxial cements: Proposed meteoric-marine mixing zone phreatic cements from Mississippian limestones, New Mexico. Journal of Sedimentary Petrology, v.48, p.475-488.

Meyers, W.J. and Lohmann, K.C., 1985. Isotope Geochemistry of Regionally Extensive Calcite Cement Zones and Marine Components in Mississippian Limestones, New Mexico. *In* N. Schneidermann and P.M. Harris, eds., Carbonate Cements, Society of Economic Paleontologists and Mineralogists, Special Publication, n.36, p.223-239.

Mii, H-s., Grossman, E.L., and Yancey, T.E., 1999. Carboniferous isotope stratigraphies of North America: Implications for Carboniferous paleoceanography and Mississippian glaciation. GSA Bulletin, v.111, n.7, p.960-973.

Moldovanyi, E.P. and Lohmann, K.C, 1984. Isotopic and petrographic record of phreatic diagenesis: Lower Cretaceous Sligo and Bupido Formations. Journal of Sedimentary Petrology, v.54, p.972-985.

Moore, C.H. and Druckman, Y., 1981. Burial Diagenesis and Porosity Evolution, Upper Jurassic Smackover, Arkansas and Louisiana. American Association of Petroleum Geologists Bulletin, v.65, n.4, p.597-628.

Mucci, A. and Morse, J.W., 1983. The incorporation of Mg^{2+} and Sr^{2+} into calcite overgrowths: influences of growth rate and solution composition. Geochimica et Cosmochimica Acta, v.47, p.217-233.

Niemann, J.C and Read, J.F., 1988. Regional Cementation from Unconformity-Recharged Aquifer and Burial Fluids, Mississippian Newman Limestone, Kentucky. Journal of Sedimentary Petrology, v.58, n.4, p.688-705.

O'Neil, J.R., Clayton, R.N, and Mayeda, T.K., 1969. Oxygen isotopic fractionations in divalent metal carbonates. Journal of Chemical Physics, v.51, p.5547-5558.

Pray, L.C., 1961. Geology of the Sacramento Mountains escarpment, Otero County, New Mexico. New Mexico Bureau of Mines and Mineral Resources Bulletin 35, 144 pp.

Rankey, E.C., Bachtel, S.L., and Kaufman, J., 1999. Controls on Stratigraphic Architecture of Icehouse Mixed Carbonate-Siliciclastic Systems: A Case Study from

the Holder Formation (Pennsylvanian, Virgilian), Sacramento Mountains, New Mexico. *In* Paul M. Harris, Arthur H. Saller, and J.A. Toni Simo eds., Advances in Carbonate Sequence Stratigraphy: Application to Reservoirs, Outcrops and Models, SEPM Special Pub. No.63, p.127-150.

Rivera, M.A., 1999. Depositional Facies Analysis of the Late Pennsylvanian, Lower Holder Formation Phylloid Algal Mound Complexes, Sacramento Mountains, New Mexico. New Mexico State University unpublished M.S. Thesis, 143pp.

Sandberg, P.A., 1983. An oscillating trend in Phanerozoic nonskeletal carbonate mineralogy. Nature, v.305, p.19-22.

Saller, A.H. and Moore, C.H. Jr., 1991. Geochemistry of meteoric calcite cements in some Pleistocene limestones. Sedimentology, v.38, p.601-621.

Soreghan, G.S., 1992. Sedimentology and Process Stratigraphy of the Upper Pennsylvanian Pedregosa (Arizona) and Orogrande (New Mexico) Basins. University of Arizona unpublished Ph.D. Dissertation, 277pp.

Soreghan, G.S. and Giles, K.A., 1999. Amplitudes of Late Pennsylvanian glacioeustasy. Geology, v.27, n.3, p.255-258.

Tobin, K.J., Steinhauff, D.M., and Walker, K.R., 1999. Ordovician meteoric carbon and oxygen isotopic values: implications for the latitudinal variations of ancient stable isotopic values. Palaeogeography, Palaeoclimatology, Palaeoecology, v.132, p.159-172.

Toomey, D.F., 1981. Organic buildup constructional capability in Lower Ordovician and Late Paleozoic mounds. *In* J. Grey, ed., Communities of the Past: Stroudsberg, Hutchinson Ross Publishing Company, p.35-68.

Toomey, D.F. and Babcock, J.A., 1983. Yucca Mound and Leopard Knob, Late Pennsylvanian Bioherms and Associated Beds, Western End of Dry Canyon, Sacramento Mountains, New Mexico. *In* D.F. Toomey and J.A. Babcock eds., Precambrian and Paleozoic Algal Carbonates, West Texas-Southern New Mexico: Field Guide to Selected Localities of Late Proterozoic, Ordovician, Pennsylvanian, and Permian ages, including the Permian Reef Complex. Colorado School of Mines Professional Contribution #11. Third International Symposium on Fossil Algae. Colorado School of Mines Press; Golden, Colorado, p.123-160.

Toomey, D.F., Wilson, J.L., and Rezak, R., 1977. Evolution of Yucca Mound Complex, Late Pennsylvanian Phylloid-Algal Buildup, Sacramento Mountains, New Mexico. AAPG Bulletin, v.61, n.12, p.2115-2133.

Veizer, J., 1983. Chemical Diagenesis of Carbonates: Theory and Application of Trace Element Technique. *In* M.A. Arthur, T.F. Anderson, I.R. Kaplan, J. Veizer, and L.S.

Land, eds., Stable Isotopes in Sedimentary Geology, SEPM Short Course, n.10, p.3-1 – 3-100.

Veizer, J., Ala, D., Azmy, K., Bruckschen, P., Buhl, D., Bruhn, F., Carden, G.A.F., Diener, A., Ebneth, S., Godderis, Y., Jasper, T., Korte, C., Pawellek, F., Podlaha, O.G., Strauss, H., 1999. $^{87}Sr/^{86}Sr$, $\delta^{13}C$ and $\delta^{18}O$ evolution of Phanerozoic seawater. Chemical Geology, v.161, p.59-88.

Whittle, G.L., Kendall, C.G.St.C., Dill, R.F., and Rouch, L., 1993. Carbonate cement fabrics displayed: A traverse across the margin of the Bahamas Platform near Lee Stocking Island in the Exuma Cays. Marine Geology, v.110, p.213-243.

Wilson, J.L., 1967. Cyclic and Reciprocal Sedimentation in Virgilian Strata of Southern New Mexico. GSA Bulletin, v.78, p.805-818.

APPENDIX I:

Geochemical Data for Individual Cement Phases

Cement Phase	Sample ID	$\delta^{13}C*$	$\delta^{18}O*$	Mg/Ca#	Sr/Ca	Fe/Ca	Mn/Ca	Sr/Mg	Stratigraphic Location (m) Distance from base of section
Cement I									
	DC04-18L-A	1.4	-7.3	10.5	0.529	1.18	0.161	0.051	5.5
	DC04-18L-A	1.3	-4.9	15.7	0.367	0.516	0.158	0.023	5.5
	DC04-18	-0.4	-5.7	7.59	0.285	3.44	0.237	0.038	6.75
	DC04-8U	1.6	-4.5	22.8	0.611	2.05	0.238	0.027	7.2
	DC04-8U	1.0	-5.5	21.2	0.376	1.14	0.213	0.018	7.2
	DC04-8U	1.6	-4.2	12.6	0.215	1.69	0.152	0.017	7.2
	DC04-8U	1.5	-4.3	18.6	0.271	1.94	0.236	0.015	7.2
	DC04-20	0.9	-4.3	10.8	0.549	0.456	0.0891	0.051	10.5
	DC04-20	1.0	-4.9	12.4	0.577	0.404	0.101	0.046	10.5
	DC04-22	0.1	-4.8	6.88	0.420	4.64	1.12	0.061	14.25
	DC04-23	0.1	-5.1	5.22	0.254	0.398	0.0573	0.049	15.5
	DC04-25	0.4	-4.8	7.76	0.302	0.273	0.0777	0.039	20.25
Cement II									
	DC04-4	3.0	-5.2	26.7	1.18	1.79	0.264	0.044	4.25
	DC04-4			33.7	1.45	0.600	0.216	0.043	4.25
	DC04-4	2.0	-5.3	29.4	0.709	1.02	0.180	0.024	4.25
	DC04-14	1.4	-5.8	16.0	0.582	0.938	0.178	0.036	4.5
	DC04-14	1.5	-5.8	14.2	0.512	1.78	0.148	0.036	4.5
	DC04-17	2.8	-6.1	31.9	0.775	0.434	0.0405	0.024	4.5
	DC04-17	2.6	-5.7	21.4	0.838	0.266	0.0370	0.039	4.5
	DC04-18L-A	1.3	-5.4	9.40	0.394	0.828	0.118	0.042	5.5
	DC04-18L-A	1.3	-6.1	7.04	0.438	0.791	0.110	0.062	5.5
	DC04-18L-B	1.2	-5.6	16.5	0.452	3.94	0.236	0.027	5.5
	DC04-18L-B	1.4	-5.6	12.1	0.424	0.269	0.126	0.035	5.5
	DC04-18L-E	1.4	-5.6	14.5	0.412	0.607	0.159	0.028	5.5
	DC04-18L-E	1.0	-5.8	13.9	0.362	0	0.325	0.026	5.5
	DC04-18	1.1	-5.4	10.1	0.346	0.936	0.167	0.034	6.75
	DC04-19	0.9	-5.4	8.12	0.415	0.699	0.0835	0.051	9.5
	DC04-20	0.7	-5.1	8.35	0.180	1.07	0.125	0.022	10.5
	DC04-20	0.9	-5.0	9.15	0.352	0.260	0.126	0.038	10.5
	DC04-25	0.2	-5.5	6.74	0.243	0.738	0.113	0.036	20.25
	DC04-26	-0.8	-5.6	4.17	0.217	0.338	0.0847	0.052	21.75

DC04-26	0.3	-5.0	5.05	0.216	0.352	0.0949	0.043	21.75
Cement III								
DC04-14	5.2	-5.2	24.0	1.40	0.346	0.0333	0.058	4.5
DC04-14	5.2	-5.0	31.2	1.44	0.0872	0.0304	0.046	4.5
DC04-17	2.2	-5.5	6.50	0.435	1.07	0.0458	0.067	4.5
DC04-18L-B	0.7	-5.9	13.5	0.326	0.936	0.113	0.024	5.5
DC04-18L-B	0.5	-5.4	6.17	0.270	0.226	0.0453	0.044	5.5
DC04-18L-B	0.1	-5.7	5.53	0.256	0	0.168	0.046	5.5
DC04-18L-C	-0.4	-5.9	5.21	0.357	0.452	0.0613	0.068	5.5
DC04-18L-D	-0.1	-5.5	7.29	0.222	0.975	0.0899	0.030	5.5
DC04-18L-D	0.0	-5.8	4.82	0.343	0.737	0.225	0.071	5.5
DC04-18L-E	0.8	-6.0	5.77	0.245	0.229	0.0251	0.042	5.5
DC04-18L-E	0.2	-5.7	6.52	0.255	0.342	0.0576	0.039	5.5
DC04-18	-0.4	-5.4	10.0	0.248	1.58	0.150	0.025	6.75
DC04-18	-0.3	-5.5	4.99	0.352	0.332	0.0911	0.071	6.75
DC04-18	-0.1	-5.4	4.99	0.352	0.332	0.0911	0.071	6.75
DC04-19	-0.3	-5.7	4.26	0.213	0.0936	0.0872	0.050	9.5
DC04-19	-0.3	-5.7	4.15	0.223	0.436	0.0741	0.054	9.5
DC04-10	-0.9	-5.7	3.42	0.157	0.351	0.0313	0.046	10.25
DC04-10	-0.9	-5.5	4.32	0.168	0.0270	0.0784	0.039	10.25
DC04-20	0.1	-5.8	3.22	0.160	0.992	0.195	0.050	10.5
DC04-20	0.1	-6.0	3.33	0.160	0.495	0.127	0.048	10.5
DC04-22	-1.1	-5.5	3.33	0.158	0.367	0.0342	0.047	14.25
DC04-22	-1.3	-5.5	3.23	0.181	0.323	0.0206	0.056	14.25
DC04-23	-0.8	-5.6	3.27	0.148	0.0448	0.0339	0.045	15.5
DC04-23	-0.9	-6.2	3.09	0.169	0.924	0.0759	0.055	15.5
DC04-25	-0.7	-5.9	3.23	0.157	0.669	0.0657	0.049	20.25
DC04-25	-0.6	-5.5	3.94	0.174	0.311	0.0583	0.044	20.25
DC04-26	-1.6	-5.3	4.07	0.113	0.223	0.0332	0.028	21.75
DC04-26	-0.9	-6.1	3.23	0.203	0.673	0.0529	0.063	21.75
DC04-29	-0.8	-5.9	4.04	0.258	0.483	0.0740	0.064	22.5
DC04-29	-0.8	-5.9	4.78	0.279	2.66	0.0943	0.058	22.5
DC04-27	-0.2	-5.5	3.78	0.172	0.541	0.0454	0.046	22.75
DC04-27	-0.1	-5.7	3.77	0.194	0.496	0.171	0.051	22.75
DC04-33	0.1	-4.9	5.75	0.870	0.448	0.0862	0.151	32.75
DC04-33	0.4	-5.3	4.22	0.200	0.560	0.164	0.047	32.75

DC04-33	0.3	-5.4	5.02	0.406	0.612	0.0871	0.081	32.75
Cement IV								
DC04-18L-A	1.2	-6.6	3.51	0.254	1.09	0.231	0.072	5.5
DC04-18L-A	0.8	-6.4	2.15	0.378	0.686	0.199	0.176	5.5
DC04-18L-B	-0.3	-5.9	5.45	0.258	0.146	0.387	0.047	5.5
DC04-18L-B	0.3	-6.4	8.38	0.273	5.58	0.666	0.033	5.5
DC04-18L-C	-0.5	-6.6	5.11	0.407	2.75	0.474	0.080	5.5
DC04-18L-C	-0.3	-6.3	4.36	0.432	2.17	0.279	0.099	5.5
DC04-18L-D	-0.3	-6.1	4.35	0.397	0.771	0.454	0.091	5.5
DC04-18L-D	-0.3	-6.4	4.22	0.560	2.16	0.571	0.133	5.5
DC04-19	0.4	-6.7	16.4	0.293	7.69	1.41	0.018	9.5
DC04-19	0.3	-6.5	6.20	0.162	3.21	1.63	0.026	9.5
DC04-29			5.94	0.448	3.13	0.653	0.075	22.5
DC04-29	-0.4	-6.2	9.15	0.335	2.20	0.957	0.037	22.5
DC04-27	0.2	-6.1	5.24	0.367	0.748	1.03	0.070	22.75
DC04-27	0.3	-6.7	5.81	0.316	4.32	1.63	0.054	22.75
DC04-30	0.4	-6.1	5.38	0.370	1.83	0.559	0.069	24.5
DC04-33	0.4	-5.9	4.37	0.310	0.425	0.146	0.071	32.75
Cement V								
DC04-17	0.9	-7.7	7.10	0.694	2.45	0.182	0.098	4.5
DC04-18L-A	2.6	-7.1	3.89	0.406	1.90	0.108	0.104	5.5
DC04-18L-A	2.4	-7.4	4.67	0.592	2.88	0.110	0.127	5.5
DC04-18L-B	1.7	-7.0	8.90	0.371	3.98	0.267	0.042	5.5
DC04-18L-B	1.2	-8.6	2.99	0.325	1.85	0.204	0.108	5.5
DC04-18L-C	0.7	-7.4	4.15	0.679	6.09	0.245	0.164	5.5
DC04-18L-C	0.2	-6.9	4.35	0.811	8.25	0.191	0.187	5.5
DC04-18L-D	0.8	-6.5	4.50	0.560	2.27	0.119	0.124	5.5
DC04-18L-D	1.2	-7.5	4.74	0.644	4.41	0.224	0.136	5.5
DC04-19	1.2	-7.5	3.00	0.197	2.31	0.337	0.066	9.5
DC04-19	1.4	-7.4	4.29	0.291	3.34	0.384	0.068	9.5
DC04-10	0.6	-7.7	4.32	0.253	3.25	0.270	0.059	10.25
DC04-10	0.6	-7.3	4.97	0.219	2.85	0.306	0.044	10.25
DC04-20	0.5	-7.3	4.52	0.219	2.84	0.369	0.048	10.5
DC04-20	0.7	-7.6	5.59	0.256	3.08	0.298	0.046	10.5
DC04-22	0.2	-7.3	3.58	0.205	2.79	0.233	0.057	14.25

DC04-22	0.4	-7.4	3.90	0.290	3.33	0.252	0.074	14.25
DC04-23	0.2	-7.5	3.86	0.212	2.89	0.229	0.055	15.5
DC04-23	0.1	-7.6	3.90	0.188	2.33	0.208	0.048	15.5
DC04-25			4.01	0.208	3.96	0.236	0.052	20.25
DC04-25	0.4	-7.4	4.77	0.190	3.64	0.236	0.040	20.25
DC04-27			7.00	0.541	6.46	0.996	0.077	22.75
DC04-27	0.7	-7.5	6.42	0.395	8.02	0.773	0.061	22.75
DC04-30	0.8	-6.6	6.84	1.01	16.3	0.199	0.148	24.5
DC04-33	0.5	-7.0	4.49	0.185	2.56	0.125	0.041	32.75
DC04-33	0.5	-7.0	4.79	0.207	2.20	0.121	0.043	32.75

*Data reported in ‰ values against VPDB
#Elemental Ratios reported in mmol/mol values

73